

REPORT



Antigenic landscapes on *Staphylococcus aureus* pore-forming toxins reveal insights into specificity and cross-neutralization

Shweta Kailasan^{a*}, Ravi Kant^{b*}, Madeleine Noonan-Shueh^a, Tulasikumari Kanipakala^a, Grant Liao^a, Sergey Shulenin^a, Daisy W. Leung^c, Richard A. Alm^d, Rajan P. Adhikari^a, Gaya K. Amarasinghe^e, Michael L. Gross^b, and M. Javad Aman^a

^aIntegrated BioTherapeutics, Rockville, USA; ^bDepartment of Chemistry, Washington University in St. Louis, St. Louis, USA; ^cDepartment of Medicine, Washington University in St. Louis, St. Louis, USA; ^dBoston University School of Law, Boston University, Boston, USA; ^eDepartment of Pathology and Immunology, Washington University in St. Louis, St. Louis, USA

ABSTRACT

Staphylococcus aureus carries an exceptional repertoire of virulence factors that aid in immune evasion. Previous single-target approaches for *S. aureus*-specific vaccines and monoclonal antibodies (mAbs) have failed in clinical trials due to the multitude of virulence factors released during infection. Emergence of antibiotic-resistant strains demands a multi-target approach involving neutralization of different, non-overlapping pathogenic factors. Of the several pore-forming toxins that contribute to *S. aureus* pathogenesis, efforts have largely focused on mAbs that neutralize α -hemolysin (Hla) and target the receptor-binding site. Here, we isolated two anti-Hla and three anti-Panton-Valentine Leukocidin (LukSF-PV) mAbs, and used a combination of hydrogen deuterium exchange mass spectrometry (HDX-MS) and alanine scanning mutagenesis to delineate and validate the toxins' epitope landscape. Our studies identified two novel, neutralizing epitopes targeted by 2B6 and CAN6 on Hla that provided protection from hemolytic activity in vitro and showed synergy in rodent pneumonia model against lethal challenge. Of the anti-LukF mAbs, SA02 and SA131 showed specific neutralization activity to LukSF-PV while SA185 showed cross-neutralization activity to LukSF-PV, γ -hemolysin HlgAB, and leukotoxin ED. We further compared these antigen-specific mAbs to two broadly neutralizing mAbs, H5 (targets Hla, LukSF-PV, HlgAB, HlgCB, and LukED) and SA185 (targeting LukSF-PV, HlgAB, and LukED), and identified molecular level markers for broad-spectrum reactivity among the pore-forming toxins by HDX-MS. To further underscore the need to target the cross-reactive epitopes on leukocidins for the development of broad-spectrum therapies, we annotated Hla sequences isolated from patients in multiple countries for genomic variations within the perspective of our defined epitopes.

ARTICLE HISTORY

Received 8 February 2022
Revised 8 May 2022
Accepted 21 May 2022

KEYWORDS

A-hemolysin; leukocidin; epitope mapping; hydrogen/deuterium exchange mass spectrometry; pneumonia; *Staphylococcus aureus*; monoclonal antibodies; MRSA

Introduction


Community-associated (CA) and hospital-associated (HA) *Staphylococcus aureus* infections are a global public health threat. *S. aureus* causes a variety of diseases from skin and soft tissue infections to life-threatening infections.¹ The emergence of methicillin-resistant (MRSA) and vancomycin-resistant *S. aureus*, which is occurring at an alarming rate, further underscores the need for continued discovery and development of novel therapeutics to counteract these "superbugs". In the United States, HA- and CA-MRSA are the most common bacteria causing skin and soft tissue infections, bacteremia, endocarditis, ventilator-associated pneumonia, as well as bone, joint, and prosthetic implant infections. To date, there are no approved vaccines or immunotherapeutics for these infections and the choice of antibiotics is becoming increasingly limited due to growing antibiotic resistance.² Vaccine and immunotherapeutic development efforts targeting MRSA infections have largely focused on surface antigens (such as IsdB, clumping factor A, lipoteichoic acid, capsular polysaccharides, and ABC transporter) to induce opsonophagocytic response, but these candidates have all failed in clinical trials,^{3–8} and one (IsdB,

Merck V710) even predisposed vaccinated individuals to more severe and lethal *S. aureus* infections.^{9,10} Animal studies also suggest that targeting surface antigens of *S. aureus* can cause deleterious CD4 T cell responses in mice leading to increased mortality.¹¹ Growing evidence, however, suggests that expression of pore-forming toxins (PFT) and superantigens directly correlates to *S. aureus* disease phenotype, while high anti-toxin antibody levels in patients correlate with better clinical outcome,^{12–15} making these virulence factors attractive therapeutic targets.

PFTs consist of a single subunit α -hemolysin (Hla) and bicomponent PFTs (BCPFT) which includes leukocidins like Panton-Valentine Leukocidin (PVL or LukSF-PV), LukED, and LukAB (also known as LukGH), and γ -hemolysins HlgAB and HlgCB. *S. aureus* BCPFTs consist of a cell-targeting S subunit (Leukocidins: LukS-PV, LukS-R, LukE, LukM, LukS-I, and LukA; γ -hemolysins: HlgA, HlgC) and an oligomerization-mediating F subunit (Leukocidins: LukF-PV, LukF-R, LukD, LukF'-PV, LukF-I, and LukB; γ -hemolysin: HlgB).^{16,17} Except for LukAB, which is released as a heterodimer, the subunits are released as inactive monomers, and the F and S oligomerize to

CONTACT Shweta Kailasan  skailasan@integratedbiotherapeutics.com  Integrated BioTherapeutics, Rockville, 20850, USA

*These authors contributed equally to this work

 Supplemental data for this article can be accessed online at <https://doi.org/10.1080/19420862.2022.2083467>

© 2022 The Author(s). Published with license by Taylor & Francis Group, LLC.

This is an Open Access article distributed under the terms of the Creative Commons Attribution-NonCommercial License (<http://creativecommons.org/licenses/by-nc/4.0/>), which permits unrestricted non-commercial use, distribution, and reproduction in any medium, provided the original work is properly cited.

enable pore formation upon receptor binding by the S subunit.¹⁸ Produced by nearly all *S. aureus* strains, Hla is secreted as a monomer that forms a pore upon interaction with its cellular receptor ADAM10.^{19,20} All subunits consist of cap, rim, and stem domains.²⁰ Of these, the stem is tightly packed against the cap but changes conformation to form a β sheet-based pore upon receptor binding, resulting in multimeric structure formation, membrane deposition, and resulting pore formation. PVL, HlgABC, and LukED have >70% sequence identity, whereas LukAB is the most divergent (<30% identity).²¹ Hla and F subunits of BCPFTs share ~27% sequence identity, but exhibit high structural homology as seen by a backbone root mean square deviation of ~0.6–1.5 Å.^{20,22} Importantly, the surface loops of Hla and all F subunits of the BCPFTs interact with the lipid bilayer on the plasma membrane and they show high sequence homology.

The majority of clinically significant *S. aureus* strains express α - and γ -hemolysins, with 30–75% of the clinical isolates also carrying LukED toxins.²³ LukAB is also prevalent in a large number of clinical isolates, but this prevalence has not been thoroughly investigated.^{24,25} Hla is expressed at higher levels in CA-MRSA than in HA-MRSA strains.^{26,27} Vaccine-based approaches that target Hla show protection from lethal pneumonia and skin infections in animal models and reduced tissue damage from pore formation, particularly in the lung tissue, in animal models.²⁸ PVL is present in 2–50% of all *S. aureus* strains depending on geographic location^{29–31} and is strongly associated with prevalent CA-MRSA lineages that have emerged worldwide in the past two decades and are most often associated with soft skin tissue infections that result in skin lesions and necrotizing pneumonia.^{32,33} PVL is often implicated in increased disease severity in healthy children and young adults compared to older patients.^{34–36}

Sero-epidemiology studies suggest protective immunity against CA and HA *S. aureus* infections in patients with higher serum levels of toxin-specific antibodies.^{37,38} Therefore, toxin-neutralizing antibody therapeutics that combat *S. aureus* infections may improve clinical outcomes. Recent studies by our group and others have described several monoclonal antibodies (mAbs) that neutralize BCPFTs and are protective in *S. aureus* rodent disease models. An α -hemolysin-targeting mAb, MEDI4893 (suv-ratoxumab), being developed by AstraZeneca (formerly MedImmune) completed a Phase 2 clinical trial (NCT02296320) in mechanically ventilated adult subjects. MEDI4893, which was generated by introducing the YTE mutations into the mAb LC10 to extend the antibody half-life, demonstrated increased survival and reduced bacterial burden in the lungs of normal and immunocompromised mice with *S. aureus* pneumonia and improved half-life pharmacokinetics.^{39,40} Another α -hemolysin-targeting mAb, CAN6 (CAN24G4-1) isolated by us and our collaborators at Cangene Corporation from hybridomas, showed highly neutralizing activity in rabbit red blood cell (RRBC) hemolytic assay.⁴¹ Unlike these mAbs, which only neutralize Hla toxin, the H5 mAb (Hla-F#5 or ASN-1; developed by Arsanis, Inc.) isolated from a high diversity human IgG1 yeast display library shows cross-neutralization activity with Hla, HlgAB, HlgCB, LukED, and LukSF-PVL.¹⁴ This mAb showed protection in rodent models but failed to show statistical significance in a Phase 2 trial (NCT02940626) where ASN-100 (cocktail of ASN-1 and ASN-2 targeting Hla and six leukocidins, respectively) was used to treat

patients who were heavily endotracheally colonized with *S. aureus* pneumonia and who were mechanically ventilated.⁴² While these studies highlight the biological significance of neutralizing antibodies, the molecular basis for neutralization remains to be defined.

Previous molecular characterization and structural studies have highlighted the rim domain of the leukocidins as one of the critical elements for pore formation and a likely target as a neutralizing epitope. Consistent with this notion, LC10⁴⁰ and H5,¹⁴ however, target an overlapping region on the rim domain, and yet only the H5 mAb shows broad cross-neutralization activity. Given the complex pathogenesis of *S. aureus* and the large number of toxins involved, it is critical to delineate the neutralizing epitopes on these toxins and to define the antigenic determinants of cross-neutralization.

In order to address this need, we took two approaches to identify potent neutralizing antibodies. Among the antibodies isolated, here we describe the characterization of three anti-LukF mAbs and two promising anti-Hla mAbs from human yeast phage display and hybridoma fusion where mice were vaccinated with Hla protein. To determine the molecular basis for broad cross-neutralization, we used a combination of epitope binning, and HDX-MS, followed by alanine mutagenesis to validate the epitopes and further understand their antigen-specificity and cross-neutralizing effect on Hla and PVL. The resulting data revealed two novel epitopes for Hla that show synergy *in vitro* and corresponding protection *in vivo* in an *S. aureus* pneumonia rodent model. While the rim domain remains a crucial neutralizing epitope, complementing treatment against *S. aureus* infection with an additional Hla mAb that targets a novel neutralizing epitope and has a unique mechanism of action, showed enhanced protection *in vivo* compared to single mAb treatments. Together, our results provide molecular-level insights into how these novel and distinct epitopes support the neutralization of several *S. aureus* toxins (Figure 1a).

Results

Novel monoclonal antibodies that neutralize LukF and α -hemolysin

Using a limited screen of a human yeast display library,⁴³ we isolated three mAbs SA02, SA131, and SA185 that show binding to LukF component of PVL toxin (Figure 1). Of these, SA131 showed the strongest binding to LukF (Half maximal effective constant (50%) (EC_{50}) = 0.025 μ g/mL) compared to those of SA02 (EC_{50} = 0.050 μ g/mL) and SA185 (EC_{50} = 0.4 μ g/mL) (Figure 1a). In addition to significant reactivity to LukF, SA185 exhibited cross-reactivity to LukD and HlgB, albeit at a reduced level (Figure 1a). These mAbs were further evaluated for their ability to neutralize toxin-mediated toxicity in induced HL60 cells that behave similar to polymorphonuclear cells (PMNs) using a previously established toxin neutralization assay (TNA) with BCPFTs PVL (LukSF-PV), LukED, HlgAB, and HlgCB (Figure 1b).³⁷ SA131 showed superior neutralization of PVL with an Inhibition constant (50%; IC_{50}) of 2.6 μ g/mL compared to SA02, which showed modest activity with an IC_{50} of ~16.5 μ g/mL (Figure 1b). Although cross-reactive mAb SA185 showed reduced neutralization activity against PVL (IC_{50} = 445 μ g/mL)

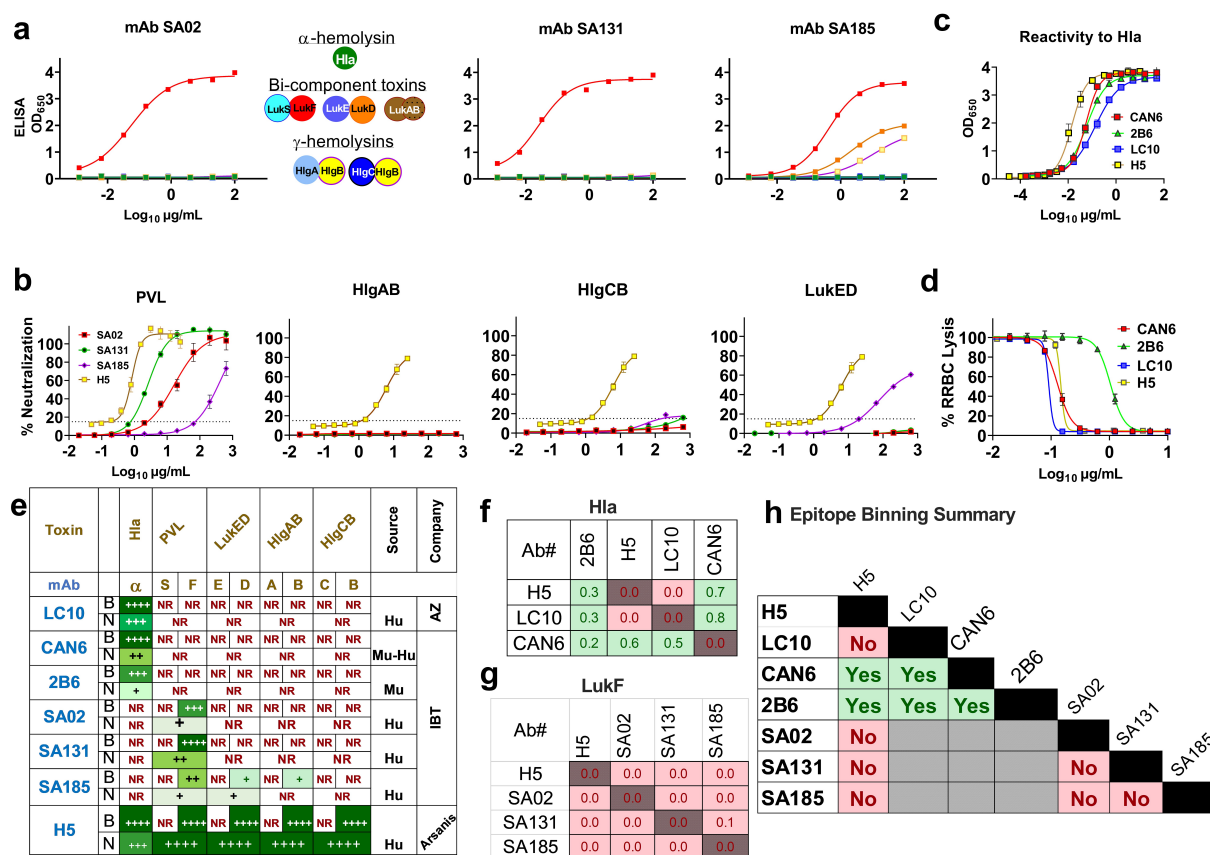


Figure 1. Characterization of newly isolated anti-LukF and anti-Hla mAbs. (a) Anti-LukF mAbs, SA02, SA131, and SA185, starting at 100 μ g/mL were titrated in semi-log fashion and tested for reactivity using LukF (red), Hla (green), LukD (Orange), HlgB (yellow with pink outline), HlgA (light blue), HlgC (blue), LukS (cyan), LukE (purple) and LukAB (brown) coated ELISA plates (1 μ g/mL) and readout was measured at OD₆₅₀. (right panel) The toxins which fall under α -hemolysins, bi-component toxins and γ -hemolysins have been shown schematically and individual components are color-coded. (b) Percentage (%) neutralization by mAbs, SA02, SA131, SA185 and H5, in HL-60 derived neutrophils treated with 25 nM LukSF-PV, 480 nM LukED, 120 nM HlgAB, or 100 nM HlgCB, and viability measured using Cell-TiterGlo. (c) Reactivity of anti-Hla mAbs to Hla coated plates (1 μ g/mL) measured by ELISA. (d) Protection from hemolytic activity of Hla WT toxin (0.42 nM) in RRBCs by anti-Hla mAbs. (e) Summary table of anti-LukF, anti-Hla mAbs and bNAb H5 describing reactivity, neutralization, antibody backbone- human (Hu) or murine (Mu), and reference company responsible for isolation and development. Epitope binning was conducted using Octet96 using classical sandwich assay format where mAb 1 (5 μ g/mL) was loaded onto anti-human/mouse FC sensors, followed by antigen association with (e) Hla (357 nM) or (f) LukF (347 nM) and loading of competing mAb (1 μ g/mL). Matrix created using Data Analysis HT 10 software by plotting the two mAbs in columns, normalizing nM shift values after subtraction of self-to-self interaction and color-coded to discriminate between a blocking (red) versus binding pair (green). (g) Summary of binning results.

compared to SA131 and SA02, SA185 also neutralized LukED up to 60% at the highest concentration tested (Figure 1b). The fact that SA02, SA131, and SA185 were identified from a single donor provides strong support for the premise that broadly neutralizing antibody (bNAb) can be identified by screening a larger number of donors. For comparison, we also expressed bNAb H5 in-house using the published sequence¹⁴ in ExpiCHO cells and observed that it neutralizes PVL (IC₅₀ of 0.8 μ g), HlgAB, HlgCB, and LukED at varying levels using our PMN TNA (Figure 1b). Unlike H5 (Figure 1c), SA185 did not react with Hla (data not shown), suggesting the presence of a distinct, cross-reactive epitope among BCPFTs.

Among the Hla mAbs, CAN6 (CAN24G-4) was discovered using hybridoma fusion technology, as described in detail elsewhere,⁴⁴ in mice immunized with *S. aureus* Hla protein. In a separate and similar effort, we isolated 2B6 from mouse hybridoma cells immunized with *S. aureus* Hla protein composed of the first 62 amino acids (referred to as AT62). Both mAbs showed specific reactivity to Hla by ELISA with EC₅₀s of ~50 ng/mL each (Figure 1c). CAN6 and 2B6 displayed higher reactivity to Hla than LC10 (EC₅₀ = 136 ng/mL), but lower binding compared to bNAb

H5 (EC₅₀ = 14 ng/mL) (Figure 1c). Neither 2B6 nor CAN6 showed any cross-reactivity to other toxins (data not shown). These mAbs were further evaluated for neutralization by testing their ability to protect RRBCs from Hla-mediated hemolysis. CAN6 displayed a neutralization profile similar to that of H5 (IC₅₀ = 146 ng/mL) with an IC₅₀ of ~130 ng/mL (Figure 1d). 2B6 neutralized Hla-mediated toxicity in RRBCs with an IC₅₀ of 1 μ g/mL and is the least potent of the Hla mAbs evaluated, whereas LC10 has the best neutralization activity (IC₅₀ of ~90 ng/mL) (Figure 1d).

Epitope binning defines key binding sites

In addition to LC10 and H5, already reported to bind and neutralize Hla with picomolar affinity,^{14,40} we discovered two neutralizing anti-Hla mAbs that, like LC10, are specific to Hla and do not react with the F components of BCPFTs (Figure 1e). Epitope binning performed using biolayer interferometry (BLI) for Hla reveals that H5 and LC10 serve as blocking pairs to bind competitively to Hla (Figure 1f). CAN6 acts as a binding pair with 2B6, LC10, and H5, indicating that it has a novel and distinct epitope

and mechanism of action (Figure 1f). Similarly, 2B6 also does not compete with other Hla mAbs, suggestive of another unique epitope (Figure 1f). BLI performed using LukF antigen revealed that SA02, SA131, SA185, and H5 all bind a similar region of the rim domain and sterically inhibit the other mAbs from associating with LukF (Figure 1e,g). Neutralizing mAb SA02 and SA131 have binding affinities (K_D) for LukF in the nM range ($K_D = 1.32$ nM and 0.52 nM, respectively) (Table S1). H5 exhibits a binding affinity to LukF within a similar range to that of SA131 ($K_D = 0.4$ nM) (Table S1). SA185 has weaker reactivity to LukF, but shows cross-reactivity to LukD and HlgB Figure 1(a,e). Altogether, the epitope binning results reveal three unique, non-overlapping epitopes for Hla and a single neutralizing epitope for LukF (Figure 1h). Furthermore, the competition between the Hla-specific LC10 and the bNAb H5 indicates a close relationship between a unique and cross-reactive epitope within the rim domain of PFTs (Figure 1h). Considering the differences seen in the neutralization profiles of the LukF mAbs, it is clear that fine differences exist within the rim epitope that differentiates LukF-specific and cross-neutralizing mAbs targeting this region.

In vivo synergy by a combination of multiple Hla neutralizing antibodies

Our initial analysis showed that CAN6 and 2B6 target non-overlapping epitopes (Figure 1f). Thus, we first evaluated the synergy between CAN6 and 2B6 *in vitro* by using the RRBC lysis assay. CAN6 or 2B6 starting at 5 $\mu\text{g}/\text{mL}$ or combination of each mAb at 5 $\mu\text{g}/\text{mL}$ were serially diluted two-fold and then added to RRBCs. We similarly compared LC10 and H5 alone or in combination with 2B6 and CAN6. After incubating at 37°C for 30 min, RRBC hemolysis was measured at OD416 nm. The results indicate that the combination of both Hla mAbs showed increased neutralizing activity (IC_{50} of 11 ng/mL)

compared to individually titrated CAN6 (IC_{50} of 24 ng/mL) and 2B6 (IC_{50} of 160 ng/mL) (Figure 2a). Addition of 2B6 or CAN6 failed to significantly enhance the neutralization activity of the rim domain-targeting mAbs, LC10 and H5 (Figure 2a).

Next, we tested whether the synergy observed for 2B6 and CAN6 can be replicated *in vivo*. For this, we used a murine model of *S. aureus* pneumonia where 6–8 weeks old BALB/c mice (female) were infected with a lethal dose of 4E8 CFU/mouse of USA300 (NRS184 strain) intranasally (IN) followed by intraperitoneal (IP) treatment with antibodies 30 min post-challenge after animals were anesthetized by instillation of isoflurane. As expected for this stringent LD_{100} pneumonia model, all vehicle/phosphate-buffered saline (PBS)-treated mice ($n = 5$) succumbed to the disease on day 1 (Figure 2b). Animals treated with 800 $\mu\text{g}/\text{mouse}$ of 2B6 ($n = 5$) or CAN6 ($n = 10$) also succumbed to infection by day 1. In contrast, animals that were treated with 400 $\mu\text{g}/\text{mouse}$ of each 2B6 and CAN6 ($n = 10$) showed 50% survival by the end of the study duration, and the mice that died showed an extended mean time to death by 2 days compared to the control group ($P < .0002$). The mice treated with 2B6 and CAN6 suffered initial weight loss between days 2 and 4 but recovered by day 10 (Figure 2c). The recovery is also captured within the clinical score definitions provided in the Materials and Methods section (Figure 2d).

Epitope mapping of LukF defines overlapping neutralization sites in the rim domain

To elucidate the epitopes of four neutralizing mAbs, namely, SA02, SA131, SA185, and H5 on LukF, we performed HDX-MS on LukF in the absence and presence of mAbs. As an approach, HDX-MS has largely been successful in epitope mapping as it provides molecular level information of the epitope using observations such as solvent accessibility,

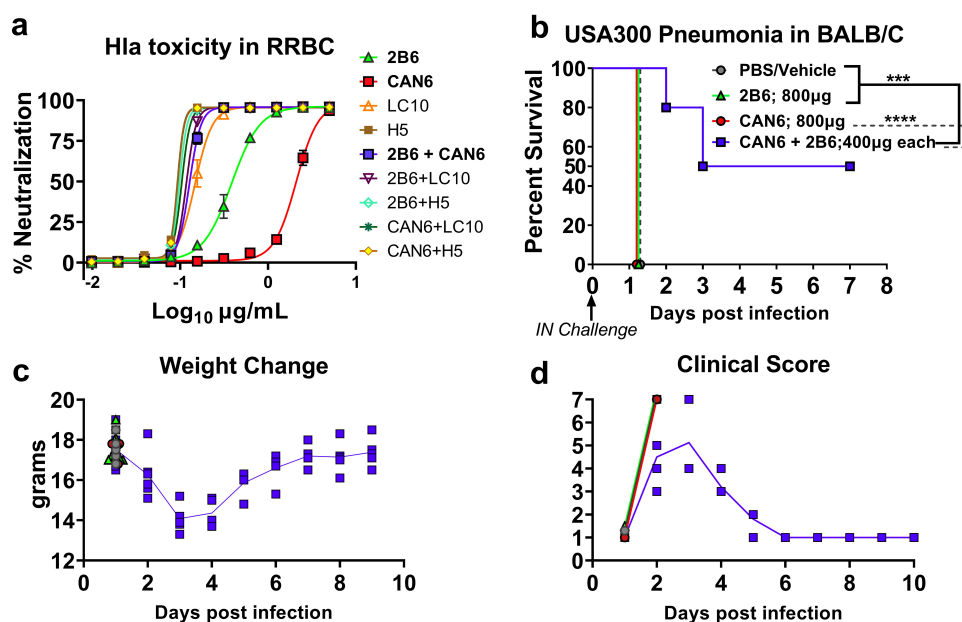


Figure 2. *In vitro* and *in vivo* synergy of 2B6 and CAN6. (a) Percentage (%) neutralization of hemolytic activity of Hla WT toxin (0.42 nM) in RRBCs by 2B6, CAN6, LC10 and H5, or combination with 2B6 or CAN6 as indicated. (b) Percentage survival plot of BALB/c mice treated with 2B6 ($n = 5$), CAN6 ($n = 10$) or combination ($n = 10$) in USA300 Pneumonia model post intranasal challenge with 4.33E8 CFU. Statistical analysis was performed using Log-Rank (Mantel-Cox) test. (c) Weight change and (d) clinical scores also compared between the groups over the course of the study for individual mice. Scoring matrix provided in methods.

hydrogen bonding, and backbone dynamics of the protein in two or more states.^{45,46} Such differences in the different protein states can provide a deeper understanding of binding, dynamics, allostery, and remote conformational changes.

Preliminary HDX measurements of LukF protein alone suggested that the protein may be classified into three groups at the 30s timepoint: group 1 (>60% HDX), group 2 (>40% HDX) and group 3 (<40% HDX) (Figure 3a). To achieve high coverage, LukF was subjected to double enzymatic digestion (Fungal protease type XIII and Pepsin), resulting in 103 unique peptides that covered the entire protein sequence (Figure S1A). Notably, several regions fell within Group 1, including the N terminus, β 1, β 5, β 6 (rim), the loop connecting β 10 and β 11 up to β 13 (stem), the rim region with a loop involving two strict beta turns (TT) located next to the strict alpha turn (TTT), the loop between η 2 and α 1 (parts of rim domain), and the C terminus (Figure 3a). These regions are less structurally ordered and/or more dynamic than regions that show little HDX at short times. The protein regions within the β -sandwich that fall within Group 3 (i.e., β 2, β 4, β 18- β 19, β 21- β 22, stem, β 10 and rim, β 16- β 17, η 1 and α 1) are either involved in strong hydrogen bonding or are buried within different inter-domain interactions (Figure 3a). The remaining parts of the stem and β -sandwich domain belong to Group 2 and show increasing HDX with time (Figure S2). Peptides that represent the majority of the rim domain show moderate to higher HDX, corroborating the dynamic nature of the rim domain of LukF. The relatively higher solvent-accessible surface areas (SASA) at the N terminus, stem domain, and C terminus, calculated using the crystal structure of LukF,⁴⁷ are consistent with our HDX results. The lack of electron density for the stem region (134–145) in the published crystal structure further substantiates its dynamic nature.

Upon SA02 binding to LukF, significant decreases in HDX occur in two regions covering A168 to Y210 and Q258 to N265 (Figure 3b, S2). The peptides representing regions A168-M192 show the largest differences: at the first time point of 30s is a diverging trend in HDX differences that continues after 1 h, suggesting strong bonding. The antigen regions showing these differences have either reduced solvent accessibility or diminished dynamics resulting from mAb binding to LukF. The peptides covering regions M192 to Y210 and Q258 to N265 show smaller differences in HDX from bound to unbound. The effects may be attenuated because the peptides are long, and localized effects are likely diluted by nearby residues that are not directly involved in the binding (Figure 3b, S2).

To further define the protected residues of LukF-SA02 complex on LukF, the cumulative deuterium differences were mapped onto the LukF crystal structure (PDB: 1PVL). The rim domain is an antiparallel, four-stranded, open-face sandwich structure made up of residues from G62-G79, K170-S218, and D250-267 K (17). The entire rim domain of LukF is protected upon SA02 binding and encompasses peptides A168-Y184 (two short beta strands β 16 and β 17 with TT), H185-M192 (TT and TTT), L194-Y210 (two TTs and η 1), and Q258-N265 (loop between β 19- β 20). While these peptides are well separated in the sequence, they are within close proximity in the crystal structure. The rim regions of G62-G79 and L208-R218, however, are unaffected by the presence of the mAb (Figure 3c, S2).

Together, these data suggest that several linear and nonlinear epitopes participate in the binding of SA02. The binding of SA131 to LukF is similar to that of SA02 (both strictly LukF-specific) but with greater differences between bound and unbound states (Figure 3(b,c), S2). The HDX data indicate that both SA02 and SA131 bind to similar linear and nonlinear epitopes on the rim domain of LukF.

Although binding of the cross-reactive SA185 to LukF causes a decrease in HDX in the bound form across the rim and β -sandwich domains, the region within the rim of A168-Y184 shows the greatest protection. In addition to the rim and unlike SA02 and SA131 mAbs, an additional region shows protection upon SA185 binding, which is located immediately upstream of the rim domain at residue Y144-A168 and includes two loops with the β -sandwich spanning β 12 to β 15 (Figure 3(b,c), S2). Therefore, the SA185 binding epitope is unique to that of SA02 and SA131 mAbs and involves residues from both the rim and β -sandwich domains.

Binding of bNAb H5 to LukF causes a decrease in HDX across different parts of the stem, β -sandwich, and rim domains. The largest differences in HDX were recorded within the rim domain for H5 when compared to those resulting from the binding of SA02 and SA131. Similar to SA185, additional protection to HDX occurs for the β -sandwich domain, β 14- β 15, located immediately upstream of the rim domain (Figure 3b,c), (S2). Therefore, the SA185 binding epitope is unique to that of SA02 and SA131 mAbs, and involves residues from both rim and β -sandwich domains. Unlike observations for SA02, SA131, and SA185, another unique range as represented by peptide G62-G79 (loop of rim domain) shows protection upon H5 binding. Altogether, our experiments suggest that the epitope of bNAb H5 is distributed not only over the entire rim domain but also includes parts of β -sandwich domain (Figure 3(b,c)). Our conclusions for the rim domain of LukF are consistent with the results of a previous crystallographic study involving a different dimeric pore-forming toxin LukAB from *S. aureus* and a monoclonal neutralizing antibody, mAb#5.H1H2 (H5).^{14,48} The investigators found that the binding epitope involves residues from different loops on the rim domain of LukB: Phe199-Lys216 (linear) and Gly64-Asn75 and Trp262-Gly269 (non-linear region).

Epitope mapping of Hla reveals two novel epitopes distinct to the well-studied rim domain

Peptide epitope mapping was used to delineate the recognition sequence of 2B6 on Hla protein. For this, 11 overlapping peptides (AT62_1-11) were generated spanning the first 62 amino acids of Hla sequence (AT62) (Figure 4a). Peptide recognition was evaluated by competition ELISA where full-length Hla protein was coated on the plate overnight at 100 ng/mL followed by incubation with 2B6 (0.5 μ g/mL) and peptides (400 μ g/mL), or 2B6 alone. Out of the 11 peptides, only AT62_5 corresponding to KTGDLVTYDKENGMH blocked binding of 2B6, confirming that it recognizes the N-terminus of Hla sequence (Figure 4b). The double enzymatic digestion (Fungal XIII and Pepsin) of Hla produced 96 unique peptides that cover the full protein sequence (Figure 5a) and allow assessment of the binding of Hla against two neutralizing antibodies, H5 and CAN6. Similar to the HDX of LukF, the

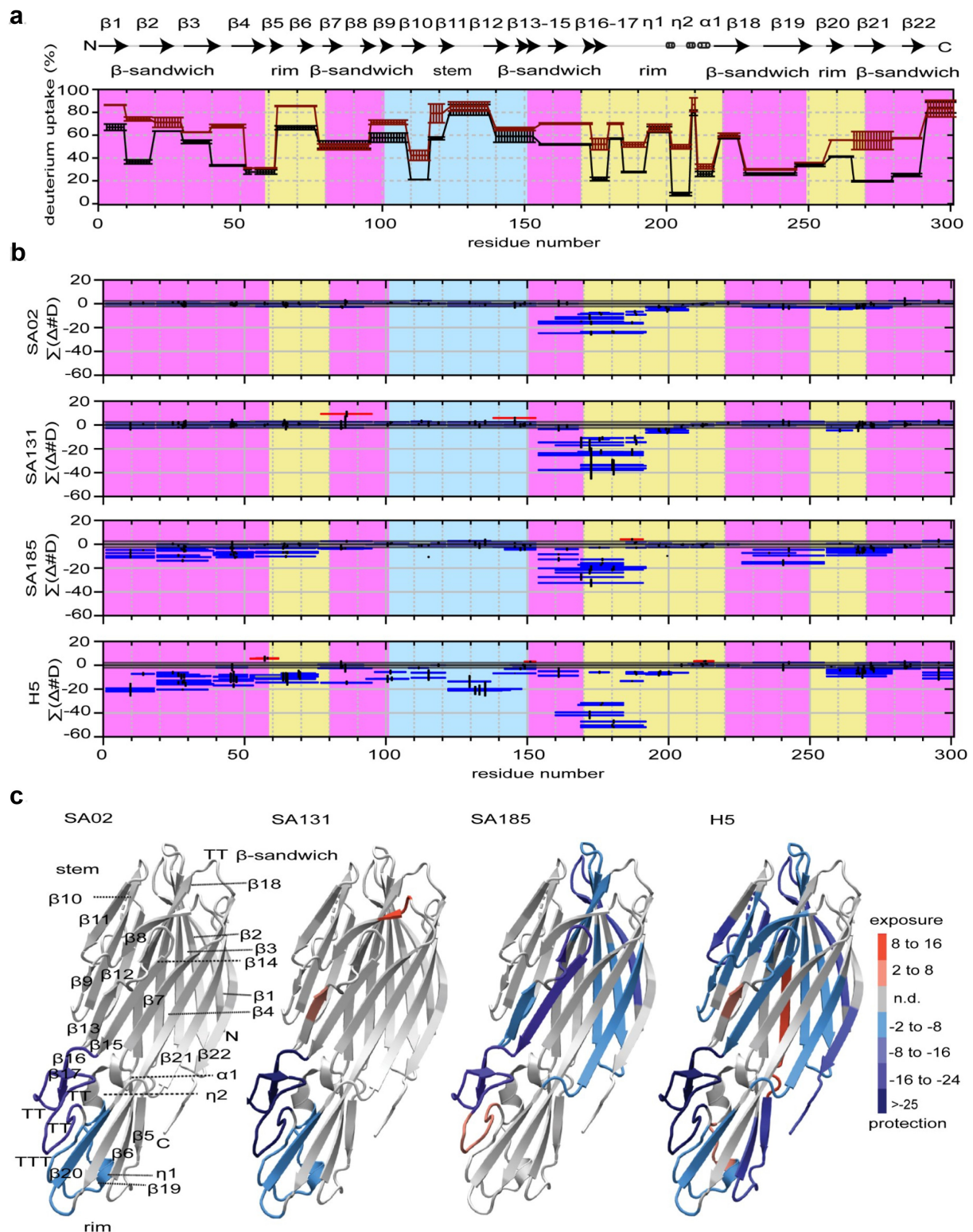


Figure 3. Epitope mapping of LukF with SA02, SA131, SA185 and H5 antibodies by HDX-MS. (a) Deuterium uptakes (%) of LukF at 30s and 1 h time scale (Y-axis) are shown as a function of residue number (X-axis). The secondary structural elements are shown on top. The secondary structures such as α -helices (medium squiggles), η helices (small squiggles), β -strands (arrows), strict α -turns (TTT), and β -turns (TT) are extracted from LukF PDB files by using ESPrpt3.0 1. The three major domains of the LukF are shown in three different colors, β -sandwich (Magenta), stem (light blue), and rim domain (light yellow). (b) Wood's plots show the cumulative HDX differences on the Y-axis (horizontal bars) and global significance limit ($p < 0.01$, the gray region with black outline). The HDX differences are calculated by subtracting the HDX of LukF from antibody bound LukF. The global significance limit is compared with cumulative differences of the peptides to assign statistically significant differences. The blue color peptides indicate significant protection, whereas the red color peptide indicates significant exposure post antibody binding. Standard deviations are shown for all the peptides. Four plots are shown with four antibodies, SA02, SA131, SA185, and H5 (top to bottom, respectively). A negative change in the cumulative differences shows potential binding sites (Y-axis). (c) The cumulative differences are mapped onto the crystal structure of LukF (PDB:1PVL) from *S. aureus*. The color key shows the statistically significant changes ranging from light to dark blue color (protection) and orange to red color (exposure) post antibody binding. The structural regions with no significant differences are shown in gray color.

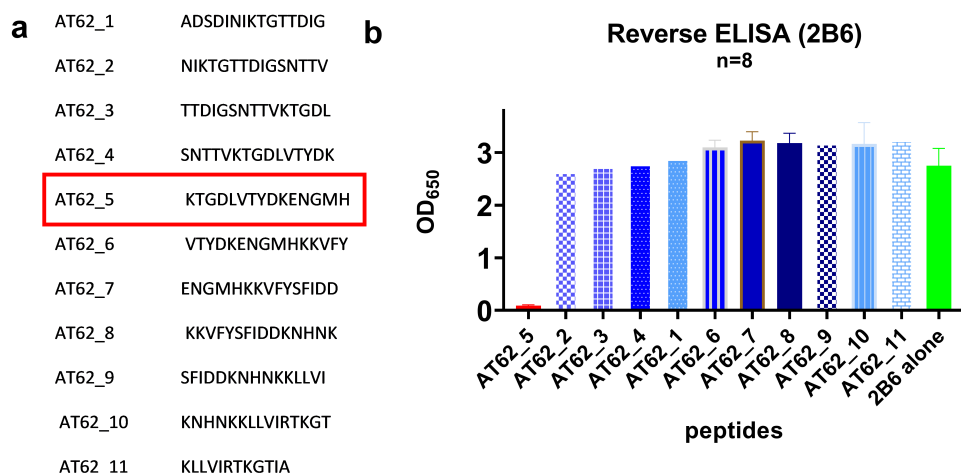


Figure 4. 2B6 peptide epitope mapping. (a) Eleven overlapping 10–15mer peptides were generated for testing covering the first 62 amino acids of Hla (AT62). (b) Reverse ELISA (n = 8) for 2B6 peptide mapping shows lack of binding to peptide AT62_5 compared to others and control 2B6 mAb alone. AT62_5 sequence highlighted in red box.

Hla structure can be classified into three groups based on the extent of HDX at 30 s. Starting with the HDX of Hla alone, we see that region 1, which includes the N-terminus (amino latch region), the loop connecting $\beta 6$ and $\beta 7$ (stem), and the rim domain adjoining alpha-helix $\eta 3$, and $\alpha 1$ undergo rapid HDX (>60%) at the earliest time point, indicating high dynamics and/or lack of structure (Figure 5a). Region 2 includes $\beta 1$, $\beta 4$ - $\beta 5$, part of $\beta 7$ and $\beta 8$ (stem), part of rim domain covering excluding $\eta 2$, and $\alpha 1$, and the mid part connecting $\beta 11$ and $\beta 12$ and undergoes moderate HDX (>40%) at the earliest time point. The remaining regions belonging to Group 3 show moderately increasing HDX over time (Figure S3). The regions showing small HDX extents are either involved in stable H-bonding or inter-domain interactions. The lack of electron density at the N terminal latch region (1–5) and a part of the stem domain (130–137) in the crystal structure⁴⁹ is consistent with the HDX, corroborating their dynamic nature.

Upon H5 binding to Hla, HDX protection occurs across the stem, the β -sandwich, and the rim domains. According to the X-ray structure, the major HDX protection occurs on the rim domain upon binding. This domain comprises both continuous (N172-P214) and non-continuous regions (A62-A79 and T261-K271), which are adjacent on the 3D structure. Significant HDX protection occurs for the whole rim domain upon antibody binding. The region represented by peptides N172-L195 shows the largest HDX differences with binding (Figure 5(b–d)). This region includes two consecutive loops composed of one alpha and three beta turns. Similar to H5 and SA185 interacting with LukF, another region on the Hla β -sandwich domain (loop connecting $\beta 9$ to $\beta 10$) upstream to N172-N214 becomes protected upon binding (Figure 5b, top panel). In summary, H5 binds via linear and nonlinear epitopes located in the vicinity of both the rim and a part of the β -sandwich domain of Hla and LukF. The HDX protection on the rim domain is also consistent with our previous epitope binning study showing that H5 competes with the LC10 (Figure 1f). A crystallographic study involving Hla and LC10 found that the antibody interacts with the rim domain and thereby exerts its neutralization effect. Those investigators also showed that the binding region is a nonlinear epitope that is composed of two segments N177-R200 and T261-K271.⁵¹

Contrary to the above observations with neutralizing antibodies tested on LukF and Hla, CAN6 binding to Hla does not occur at the rim, as seen by a lack of significant HDX protection. In fact, significant increased exposure is seen in the rim domain, specifically the C-terminal half of $\beta 12$, $\beta 13$, as well as $\beta 12$ - $\beta 13$ and $\beta 13$ - $\beta 14$ loops, indicating conformational changes in the rim domain. On the other hand, the largest differences in HDX occur in the loops connecting the C-terminal side of $\beta 11$, the N-terminal side of $\beta 12$ (M234-V247), and the C-terminal side of $\beta 14$ on to the N-terminal side of $\beta 15$ (R281-N293) (β -sandwich domain) (Figure 5(c,d)). Thus, the CAN6 epitope is different than those of SA02, SA131, SA185, and H5 because they show binding nearer the C-terminus (β -sandwich domain). Although the full sequence of both Hla and LukF only share ~27% identity, the rim domain (177–200) of Hla shares 55% sequence identity including conserved residues,¹⁴ e.g., N176, W179, G180, P181, Y182, R184, D185, S186, Y191, G192, N193, R200, D254, Y256, W260, W265, N269, and K271. Irrespective of the toxin, HDX shows that the antibodies (SA02, SA131, and H5) interact with the conserved part of the rim domain and exhibit a neutralizing effect.

Antibodies induce distinct structural perturbations

With the exception of 2B6 and CAN6, the antibodies bind preferably to the rim domain of the respective toxins. There are, however, important structural changes occurring in other domains. For example, SA131 and SA02 share similar epitopes on LukF, but SA131 perturbs the structure in regions located distally from the binding epitopes. Interestingly, SA131 binding to LukF induces an increase in HDX at $\beta 8$ and C-terminus of $\beta 6$ (part of the β -sandwich domain); these changes are assigned as remote conformational changes that occur upon antibody binding. The binding of SA02 and SA131 to LukF gives rise to no significant decreases in HDX outside the rim domain, whereas both SA185 and H5 show differences (both protection and exposure) outside the rim domain. For SA185 binding to LukF, the protected regions outside the rim domain are the N-terminus, $\beta 1$ - $\beta 3$, $\beta 18$, and $\beta 21$. The exposed region, however, is an alpha-turn on the rim domain. Similarly, H5

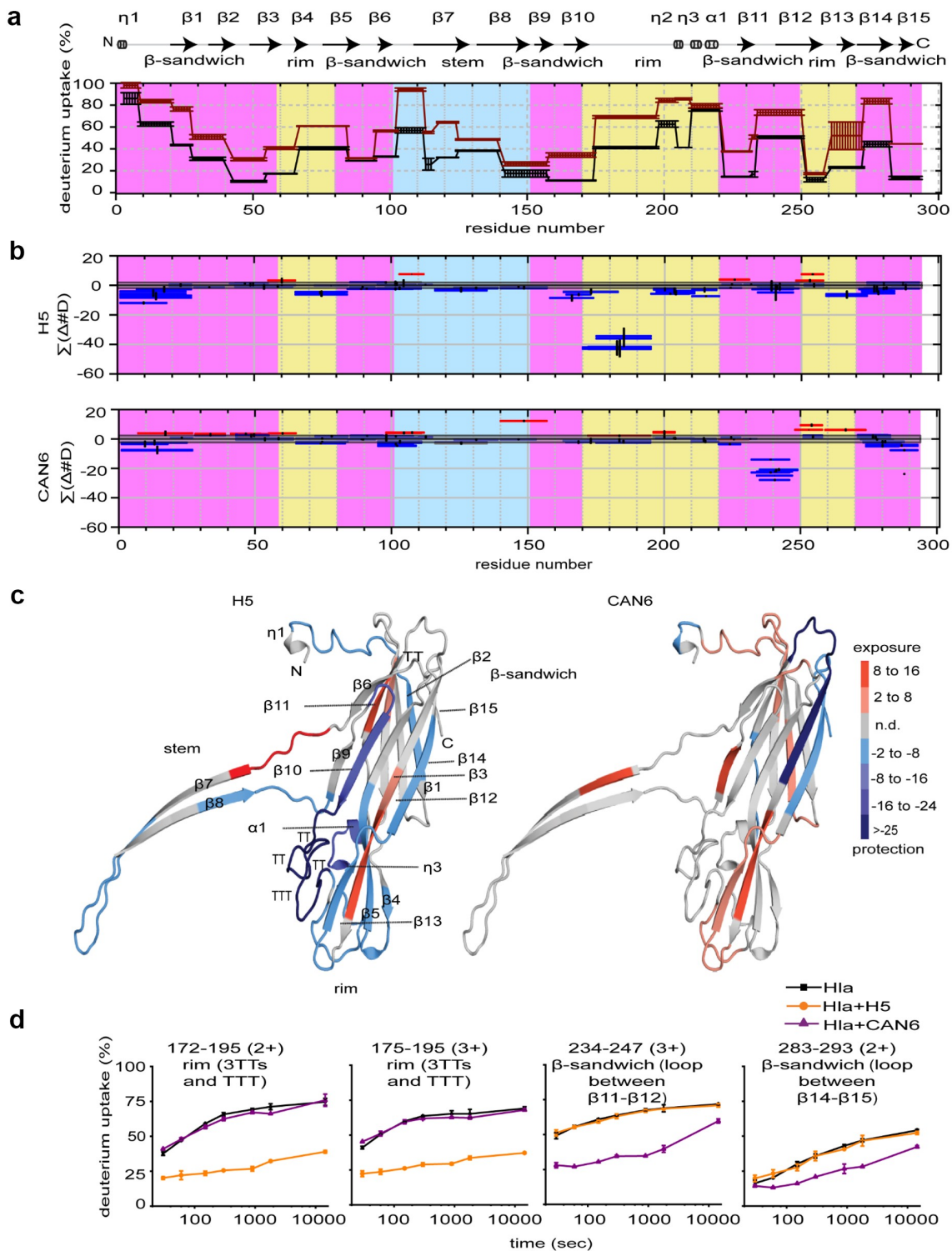


Figure 5. Epitope mapping of Hla with H5 and CAN6 antibodies by HDX-MS. (a) Deuterium uptakes (%) of Hla at 30s and 4 h time points (Y-axis) are shown as a function of residue number (X-axis). The secondary structures are shown on top. The secondary structures such as α -helices (medium squiggles), η helices (small squiggles), β -strands (arrows), strict α -turns (TTT), and β -turns (TT) are extracted from Hla PDB file (7AHL) using ESPrpt3.0 ¹⁵⁰. Three domains colored are β -sandwich (magenta), stem (light blue), and rim domain (light yellow). (b) Wood's plot shows the statistically significant differences in Hla against two antibodies, H5 (top) and CAN6 (bottom). The Y-axis (horizontal bars) is compared with the global significance limit ($p < .01$, the gray region with black outline). The global significance limit is compared with cumulative differences of the peptides to assign statistically significant differences. The HDX differences are calculated by subtracting the HDX of Hla from that of antibody-bound Hla. A negative change in the cumulative differences shows protection or the potential antibody binding sites (Y-axis). Standard deviations are shown for all the peptides. (c) The statistically significant cumulative differences are mapped on the monomer extracted from heptameric structure (PDB: 7AHL) from *S. aureus*; H5 (left) CAN6 (right). The color key shows the statistically significant changes ranging from light to dark blue color (protection) and orange to red color (exposure) upon antibody binding. The structural regions with no significant differences are shown in gray. (d) Kinetic uptake of some of the peptides representing the distinct binding sites of H5 (rim domain) and CAN6 (β -sandwich domain toward C-terminus) on Hla.

binding to LukF induced more HDX protection than for SA185. Besides, additional HDX protection occurs at stem domain, whereas exposure (structural opening) characterizes the middle of $\beta 4$, $\beta 13$, and the loop between $\eta 1$ and $\eta 2$ of the rim domain (Figure 3c).

Similar to LukF, structural perturbations occur in Hla upon binding of H5 as seen by HDX protection at the N-terminus, $\beta 1$, $\beta 9$, $\beta 10$ (stem domain), whereas exposure occurs for the loop connecting $\beta 6$ and $\beta 7$, and parts of $\beta 11$ and $\beta 12$. With CAN6 bound to Hla, minor HDX protection occurs at the N-terminus, whereas exposure is at the loops between $\beta 1$ and $\beta 2$, $\beta 2$ and $\beta 3$, part of $\beta 12$ and $\beta 13$, and rim domain (Figure 5c).

Alanine mutagenesis delineates site-specific and cross-neutralizing epitopes on Hla

To investigate the specific residues that are central to the binding of the bNabs and/or mono-toxin-specificity of the mAbs, we generated alanine mutations of selected residues within the two loops that are part of the rim domain that were identified to be critical to the various epitopes as indicated by HDX and previous literature on Hla toxin.⁵² We demarcated residue R184-S186 as Site I, which are conserved in all other F subunits of BCPFTs except for LukB of LukAB (Figure 6a). Site II includes residue Y191-R200 where more variation is seen within the sequences among the BCPFTs (Figure 6a). Of these, alanine mutagenesis was performed on Y191-N193, which participate in mAbs H5 and LC10 epitopes and are conserved in all F subunits for LukB (Figure 6a). We also mutated R200, which is conserved across all toxins at this position, and was previously shown to be important for

mAb H5 activity (Figure 6a). Lastly, we mutated W265A, which is conserved across Hla and all BCPFTs including LukAB. Our HDX experiments highlight the region containing this residue is part of a tertiary site (T261-N269) that also shows some protection from HDX at the corresponding site on LukF with the SA-mAb series (Figures 6a and 3b).

The Hla alanine mutations were produced in *E. coli* similar to wild-type (WT) and evaluated for their potential to cause toxicity in RRBCs. The RRBC lysis assay indicated that mutations within Site I retained toxicity levels similar or close to that of the WT protein (Figure 6(b,c)). The mutations that affected toxicity the most are within Site II, namely Y191A, G192A, R200A, and tertiary site W265A. These alanine substitutions caused between 5- to 80-fold reduction in toxicity compared to those in the WT (Figure 6c). Mutant N193A behaves similar to WT with a toxicity of IC_{50} of 48 ng/mL (Figure 6b). We then used these mutants to characterize the different Hla mAbs (CAN6, 2B6, LC10) and bNab (H5) for impact on reactivity by ELISA. None of the mutations affected 2B6 and CAN6 binding, which is consistent with the HDX and epitope binning results as these mAbs are non-rim binders and do not compete with H5 or LC10 (Figures 2 and 3).

The reactivity of R184A with LC10 demonstrates an unusual binding curve with reduced OD_{650} at the highest concentration compared to WT but continues to show low levels of reactivity at low concentrations of the mAb (Figure 6f). Mutation D185A within Site I has a mild impact on LC10 binding when compared to the WT binding profile (IC_{50} of ~ 0.35 $\mu\text{g/mL}$) (Figure 6f). Mutations R184A and D185A also reduce optimal binding to bNab H5 at the highest concentration tested (10 $\mu\text{g/mL}$) and an overall reduction in IC_{50} by ~ 10 -fold (Figure 6g). On the other hand, an S186A mutation of Hla enhances

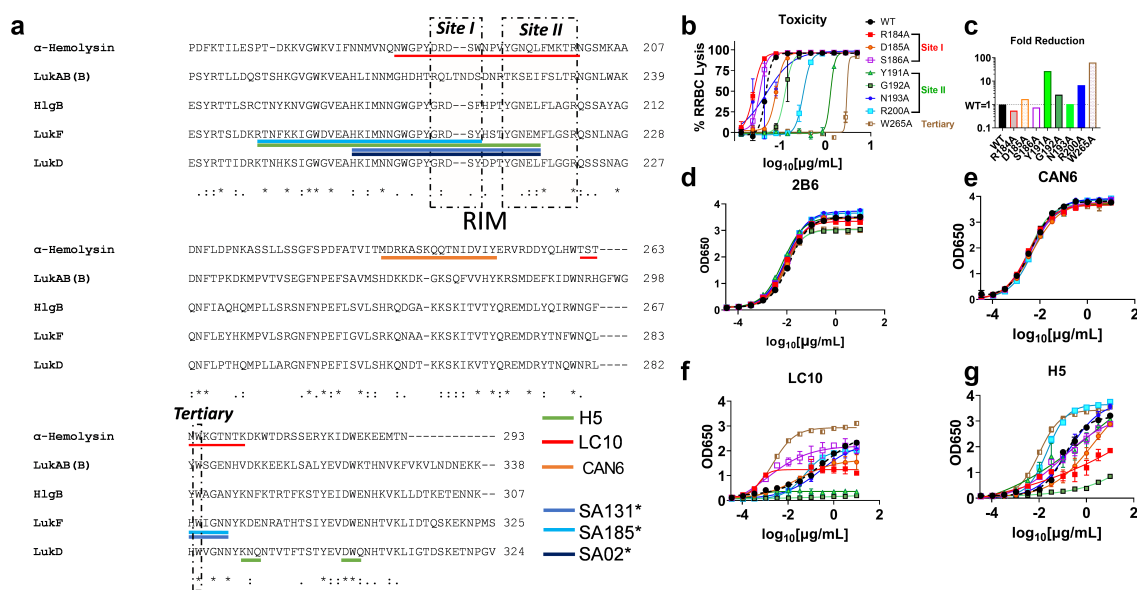


Figure 6. Characterization of Hla epitopes by alanine mutagenesis. (a) Partial sequence alignment view of Hla and B components of BCPFTs created using CLUSTALOmega highlighting the various anti-Hla, anti-LukF and bNab epitopes as per the color key. Additional regions within rim domain are demarcated with dashed lined boxes as Site I, Site II, and Tertiary. (b) Toxicity profile of the various alanine mutations in Hla toxin made within Site I, Site II, and Tertiary by using RRBC lysis assay. Percent (%) RRBC lysis shown as a function of log concentration of toxin. (c) Fold reduction calculated using ratio of EC_{50} or 50% toxicity titer of WT to that of mutant. Dotted line indicates EC_{50} ratios equal to WT. Reactivity (OD_{650}) of (d) 2B6, (e) CAN6, (f) LC10 and (g) H5 to Hla alanine mutants measured by ELISA. Y axis is shown as log of concentration ($\mu\text{g/mL}$). Toxicity and ELISA curves analyzed using 4-PL fit using PRISM.

binding to LC10 by ~350-fold with an IC₅₀ of 0.001 µg/mL, but the effect is similar to that of the WT for bNAb H5 (Figure 6(f,g)). Site II mutations, Y191A and G192A, have the most impact on LC10, resulting in complete loss of binding (Figure 6f). For bNAb H5, the Y191A mutation has no impact on binding, whereas G192A causes significant reduction but not complete loss of binding like it does with LC10 (Figure 6(f,g)).

Another Site II residue, N193A, demonstrates little to no impact on LC10 or bNAb H5 reactivity (Figure 6(f,g)). Alanine mutation at R200, a distal residue within Site II, has a similar binding profile to WT for mAb LC10 but showed enhanced reactivity to bNAb H5 by five-fold⁵² (Figure 6(f,g)). On the other hand, substitution of the bulky tryptophan with alanine at position 265 causes reactivity to both LC10 and H5 to increase by 175- and 12-fold, respectively (Figure 6(f,g)). Combined with the observation that W265A severely affects toxicity, these data suggest that W265 plays a role in mediating Hla toxicity (Figure 6(b,f,g)). Overall, our observations suggest that Site II residues such as Y191 and G192 have more impact on Hla-specific mAb LC10 than the bNAb H5, highlighting a primary difference in their binding profiles allowing H5 to facilitate cross-reactivity and cross-neutralization.

Sequence variation affects neutralizing epitopes among clinically relevant *S. aureus* isolates

To understand the level of variation in the *S. aureus* Hla toxin across a variety of isolates, especially those from low- and middle-income countries (LMIC), and its impact on the various neutralizing epitopes on Hla, we analyzed genome sequences (complete or contig lists) from a collection of isolates that were recently published in Tabor *et al.*⁵³ and others available through the Combating Antibiotic-Resistant Bacteria Biopharmaceutical Accelerator (CARB-X), a global nonprofit partnership accelerating antibacterial products to address drug-resistant bacteria. Altogether, we analyzed 970 *S. aureus* isolated by Tabor and 403 from the CARB-X database. Of the CARB-X dataset, only nine isolates lacked Hla sequence; however, it is not known whether this represents a true absence of the gene or incomplete sequence (as many strains are a compilation of assembled contigs rather than a complete chromosome). The remaining 393 isolates were from 61 countries and included 224 isolates (57%) from 38 LMICs. In total, there were 30 different Hla genotypes, including two Types XX1 and XX2 (Table 1) that had in-frame stop codons causing premature truncations, and another, Type Z, that had one base pair (bp) deletion at the 3' end leading to truncation of the last three residues. Frameshift mutations in nine isolates were also observed, and these isolates were grouped with the genotype assuming no frameshift and specifically noted. In addition, the sequence in five isolates extended off the end of a contig; if no other variation was noted, these isolates were also grouped into the closest genotype and specifically noted. There were 15 singleton Hla genotypes, and three variants with two representatives (Table 1). The distribution of the isolates across these Hla genotypes from the combined dataset is shown in Table S2. Of the 1363 isolates, 43% (n = 588) carried the Type A sequence. A total of 1092 isolates, or 80%, were represented by the 5 most prevalent sequences (Types A, B, C, D, and G; see

Table 1. Hla genotypes and the number of isolates containing that sequence from the CARB-X analysis set.

Type	Number	Type	Number
Type A	187	Type P	1
Type B	40	Type Q	1
Type C	47	Type R	2
Type D	21	Type S	1
Type F	6	Type T	1
Type F	11	Type U	1
Type G	31	Type V	1
Type H	6	Type W	1
Type I	4	Type X	1
Type J	7	Type Y	1
Type K	3	Type Z	1
Type L	2	Type AA	1
Type M	2	Type AB	1
Type N	1	Type XX1	9
Type O	1	Type XX2	1

Notes: In Type A there were 4 isolates with frameshifted sequences (three at position 190, and one at position 84) and two isolates extended off the end of the contig after position 315 (total protein length = 319 residues). In Type B there was an isolate with a frameshifted sequence at position 206. In Type D, there were 4 isolates with frameshifted sequences (two at position 97 and one at both positions 62 and 76) and one isolate whose sequence extended off the short contig at both ends (position 1–4, and >280 were missing). In Type G and Type R there was one isolate whose sequence position 1–17 and >309 extended off the contig, respectively.

Table 1). Unlike Hla, Tabor *et al.* reported the presence of PVL in 67/403 (17%) of the isolates in the CARB-X dataset, and that the LukF protein was 100% identical across all of these isolates.

We then analyzed the position of the identified variations within Hla protein sequence, combining information from both the CARB-X analysis set and that published by Tabor *et al.* (Figure 7a)⁵³. It should be noted that the Cluster 54 information from Tabor was excluded as this represents the closely related *S. argenteus* species rather than *S. aureus*. We then investigated whether these variations cluster within Hla neutralizing epitopes (Figure 7a). For this, PDBPisa was used to identify the exposed residues within Hla toxin (PBD: 7AHL) and the variations that were either solvent-exposed or at inter-monomeric interfaces (Figure 7b). Percent conservation was also determined for the 51 different isolates and represented as a worm diagram using Chimera⁵⁴ with the thickest parts of the structure representing the most conservation (Figure 7c). Among these, two of five variations were solvent accessible and within the epitope for 2B6, which is near the amino latch. The residue D28 is 97% conserved at this site with Type AB isolates having in this position a tyrosine, which may affect binding to this region (Figure 7c). The other residue S29 is 95% conserved, and Type F isolates have a threonine that may not be so detrimental (Figure 7c). There are several variations within the rim region that may affect the binding of LC10, CAN6, and H5 mAbs (Figure 7(a,b)). Between residues 197–240, there are 13 variations including frameshift mutations, suggesting that this region is subject to mutation as *S. aureus* spreads and replicates (Figure 7a). Within this residue stretch is Site I, R210-S212 (Figure 7a) (R184-S186 according to PDB structure numbering (Figure 7b; insert)), and some of the Site II residues (Y217-N219 (Figure 7a)) (Y191-N193 structure numbering (Figure 7b; insert)) that act as determinants of specificity and cross-neutralization. Site I is subjected to relatively low pressure for mutagenesis, with the sequences conserved 100% in all isolates (Figure 7c). Within Site II, the G192 position showed 97% conservation but had a valine substitution within Cluster 10

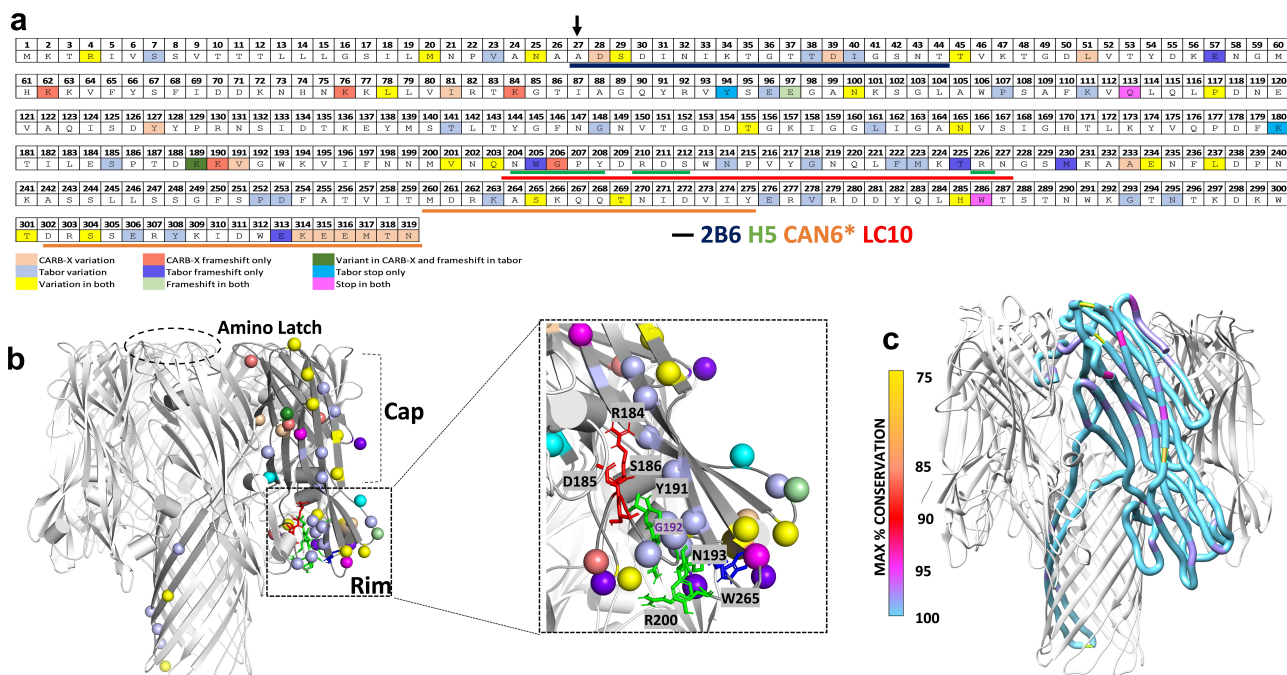


Figure 7. Hla sequence variation in clinically relevant *S. aureus* isolates and its impact on neutralizing epitopes. (a) Variations and frameshifts seen in Hla sequences deposited in Tabor *et al.* and CARB-X databases with Hla epitopes overlaid within colored underlines. Arrow indicates residue numbered 1 in deposited Hla structure (PDB: 7AHL). (b) Cartoon structure of octameric Hla ring with C-alphas of solvent exposed residues with variations highlighted as colored spheres. Color key similar to Figure 7a. Domains within Hla are labeled. (*Insert*) Zoom-in view of rim domain highlighting Site I (red sticks), Site II (green sticks) and tertiary (blue sticks) alanine mutations described in Figure 6. (c) Worm diagram generated using Chimera for one of the Hla monomers where the radii of the cartoon representation corresponds to percent maximum sequence conservation (color key provided) calculated using Clustal Omega³⁵.

(Figure 7c). Our experiments show that G192A mutation was not tolerated by LC10 and reduced binding of H5, indicating that this position is crucial to retaining Hla neutralizing activity. Although Y191A also affected LC10 binding, this position was 100% conserved among the Hla isolates, suggesting less variation for this position. Others, R226 (R200 structure numbering) and W291 (W265 structure numbering), showed 100% conservation among the different Hla isolates. Although few mutations were observed within known epitopes and reported in this study, several variations are found within the rim domain and may affect the binding of future mAbs.

Discussion

Here, we described the characterization of two novel Hla antibodies and three LukF neutralizing antibodies. Additionally, we reported two novel epitopes mapped by HDX-MS on Hla that were protective in a pneumonia rodent challenge model. We also characterized a cross-neutralizing epitope on Hla and LukF at a molecular level. HDX, which reports on solvent accessibility, hydrogen bonding, and backbone dynamics, can delineate the epitope on the toxin proteins.^{45,46} The combined data define the neutralization landscape of *S. aureus* toxins.

Several antibodies described in the literature such as MEDI4893 and ASN100 that are specific to neutralizing Hla toxicity by targeting the rim domain and involved in blocking the assembly of a heptameric complex of destabilization²⁰ at the pre-pore stage are currently in clinical trials.⁵⁶ Although the rim is

a critical site for toxin neutralization, using mAbs 2B6 and CAN6 we identified two new epitopes that mediate potent neutralization of Hla. We showed that 2B6 targets a linear epitope near the amino latch of Hla at the N-terminal region that undergoes a conformational change and allows the β -barrel pore formation from the pre-pore form.⁵⁷ Owing to the role of the amino latch in interprotomer stabilization and pore formation, we conclude the binding of 2B6 hinders this conformational change, resulting in the inactivation of the toxin.⁵⁸ These findings also corroborate our previous report that shows polyclonal antibodies raised against an experimental Hla vaccine consisting of the N-terminal 62 amino acids (AT62) effectively inhibit heptamerization of Hla.⁵⁹ CAN6 also highlights two loops of the β -sandwich domain, which is located close to the C-terminus (β 11- β 12 and β 14- β 15), as binding sites. Furthermore, dynamics at the stem, rim, and sandwich domains increased after CAN6 binding, demonstrating that the antibody binding perturbs the native structure. A decrease in dynamics near the N-terminus and rim domain is also likely to interfere with interprotomer stabilization and pore formation. Overall, we suggest that these remote conformational changes upon CAN6 binding are responsible for Hla toxin neutralization. Complementing our HDX results are the observations from alanine scanning mutagenesis experiments, highlighting antigen-specific and cross-neutralizing epitopes at the residue level of Hla. In addition to R200A, which was reported to affect hemolytic activity,⁶⁰ residues Y191A and W265A also diminished Hla-induced lytic activity. Substitution of these bulky residues for alanine provides better access and binding of the rim-targeting

bNAb H5. In contrast, Y191A substitution severely affected binding of Hla-specific mAb LC10, but not bNAb H5. Together, these data suggest that the molecular mechanism with which the bNAb blocks Hla toxicity by targeting rim residues is unique compared to the Hla-specific mAb LC10.

Our data also suggest that there are other unique epitopes on the rim domain of Hla that contribute to protection. It was shown that LC10 and H5 at doses of ~45 mg/kg when administered prophylactically 24 h prior to USA300 challenge afford up to 90% protection from pneumonia in C57BL/6 J mice.³⁹ Interestingly, 2B6 and CAN6 showed synergy *in vitro* and *in vivo* in BALB/c USA300 pneumonia challenge study where a single antibody at 800 µg dose (~40 mg/kg) failed to protect, whereas the combination of 2B6 and CAN6 at 400 µg dose per antibody showed 50% efficacy at the study endpoint. These data indicate that the two antibodies complement each other, and that targeting these epitopes individually does not provide protection from death in a murine pneumonia model.

Despite low overall sequence identity (27%) between Hla and LukF, the rim (177–200) of Hla does share 55% sequence identity with LukF.²⁰ Both SA02 and SA131 antibodies bind to the rim of LukF, as determined by HDX. As the rim domain interacts with the host cell receptor and is important for toxin oligomerization,^{61,62} it is not surprising that their recorded IC₅₀ values are small. Although both have similar epitopes, SA131 exhibits higher neutralization activity toward LukF than SA02. In contrast to SA131 and SA02, SA185 only interacts with a smaller region within the rim. Furthermore, a detailed comparison of the HDX protection on the rim suggests that the two loops from S183-E191 (involving alpha strict turn) and Q258-N265 are bound by both SA131 and SA02, but not by SA185. The lack of binding to these two loops on the rim may be responsible for a relatively lower efficiency of toxin neutralization by SA185. Therefore, rim regions S183-E191 and Q258-N265 are likely a critical site for function of a highly efficient neutralizing antibody. The LukF structure is also more dynamic upon SA131 than SA02 binding. In contrast to SA131 and SA02, SA185 can bind both the rim and a part of β-sandwich and also decrease LukF dynamics. Overall, remote conformational changes mediated by SA185 are distinct and opposite in comparison to those observed for SA131 and SA02. Both cross-reactive antibodies, SA185 and bNAb H5, have epitopes that likely span the β-sandwich in addition to the rim domain. To our knowledge, this is the first molecular-level study that identified both mono- and cross-neutralizing epitopes on LukF and accompanying allosteric effects. Binding of these mAbs to LukF may result in structural changes that affect receptor interaction and oligomerization on the cell surface, but this requires further evaluation.

In addition to HDX, alanine scanning mutagenesis was done to delineate mono-specific and cross-neutralizing epitopes on a residue level for Hla. These studies revealed that some residues (Y191 and G192) within the rim have more impact on Hla-specific antibodies than bNAb H5. These residues also affect Hla toxicity significantly and provide rationale for toxicity displayed by *S. aureus* toxins.

Our analysis of clinically relevant Hla sequences from the CARB-X database and Tabor *et al.*⁵³ also pinpoint several variations within rim mutations, especially at position G192,

suggesting that the efficacy of mAbs like LC10 may be affected if the prevalence of such isolates increases. Interestingly, no variation was reported for amino acids R226 (R200 structure numbering) and W291 (W265 structure numbering) that strongly affected Hla toxicity; removal of these bulky residues significantly enhanced the binding of bNAb H5. Our observations suggest that such residues are critical for maintaining Hla toxicity, and that antibodies interacting with these amino acids may exhibit superior neutralization activity. Moreover, these residues are also conserved in other F components of BCPFTs, and further evaluation is required to validate their roles in mediating toxicity in appropriate cell-based models.

The findings from this study extend our knowledge of the various neutralizing epitopes on PFTs beyond the rim domain and provide molecular insight on the regions that contribute to broad-spectrum neutralization and toxicity. These observations further underscore the need to understand toxin neutralizing epitopes on a molecular level to pinpoint regions that may be targeted by future discovery efforts for the simultaneous deactivation of multiple toxins. Given that *S. aureus* is a highly complex pathogen that requires a multi-target approach, an antibody cocktail against more than one class of virulence factors with a broad neutralization ability could prove to be effective as prophylactic or therapeutic counter measures.

Materials and methods

Cell culture and strains

ExpiCHO-S cells cultured in ExpiCHO Expression Medium (Thermo Fisher Scientific) in a shaker incubator set at 135 rpm, 37°C and 5.0% CO₂ were passaged and transfected as per manufacturer's recommendations.

Isolation of novel Hla and LukF antibodies

Details of the isolation of CAN6 from mouse hybridoma have been described previously.⁴⁴ In a separate effort, 2B6, SA02, SA131, and SA185 were isolated from the same mouse hybridoma cells. Sequences of heavy and light chains of CAN6, 2B6, SA02, SA131, and SA185 were cloned into pSF vector and expressed in ExpiCHO™ (ThermoFisher) cells by transient transfection and purified using protein A resin by affinity chromatography.

Leukotoxin neutralization assay

The Leukotoxin neutralization assay was performed as previously described using induced HL-60 cells (ATCC, Manassas, VA) using dimethyl sulfoxide (DMSO).³⁷ Assay details are provided in the Supplemental Appendix.

RRBC hemolytic and neutralization assay

Rabbit blood was obtained from Colorado Serum Company. Hemolytic assays were performed as previously described.⁵⁹ Assay details are provided in the Supplemental Appendix.

Antibody production in ExpiCHO

Plasmids encoding the IgH and IgL of the different antibodies were cloned into p-SF vector, which also encodes for the constant region of human IgG1. For H5 and LC10, antibody sequences were downloaded from GenBank^{14,39} and were transiently transfected into ExpiCHO-S cells (Thermo Fisher Scientific) by using ExpiFectamine CHO (Thermo Fisher Scientific) by the manufacturer's recommended protocol and cells were harvested 14 d post-transfection in a shaker incubator set at 135 rpm, 37°C, and 5.0% CO₂. The mAbs were purified using a standard protein A column (GE Lifesciences). Purity and integrity of the final product were evaluated using SDS-PAGE and SEC-HPLC.

Binding and competition ELISA

MaxiSorp™ 96-well plates (Cat: 44-2404-21) were coated with 1 mg/mL each of WT toxins LukF, LukD, HlgB, Hla, or LukAB overnight at 4°C. The following day, the plates were blocked with Starting Block buffer (SB) (ThermoFisher) for 1 h at room temperature. Antibodies titrated in SB were added to the wells and incubated for an hour at room temperature followed by incubation with an appropriate secondary detection antibody conjugated to horseradish peroxidase (Anti-Human IgG (H + L) (Cat: SeraCare 5450-0009) or Anti-Mouse IgG (H + L) (Cat: SeraCare 5450-0011)) for hour. In between each of these incubation steps, a wash cycle comprising three individual washes was carried out with 300uL of PBS-0.05%Tween using a plate washer (BioTEK ELx405). After the final wash, the plates are incubated with TMB substrate (SeraCare) for 30 min and read at an optical density of 650 nm using the VersaMax™ plate reader.

Animal studies

S. aureus pneumonia rodent models were developed at Integrated BioTherapeutics, Inc. as previously described.⁶³ Rodent work was performed with protocols approved by the Institutional Animal Care and Use Committees (IACUC) of Noble Life Sciences (OLAW registration number is A4633-01) under IACUC (14-04-027IBT). Six-to-eight-week-old female BALB/c mice (Charles River) were intraperitoneally administered on Day 0 with 2B6 (800 µg; 47 mg/kg), CAN6 (800 µg; 47 mg/kg), combination of both (400 µg each mAb; 23.5 mg/kg each) or vehicle (PBS) and intranasally infected 30 min prior to treatment with USA300 (NRS348 strain) (4E8 CFU in 50 µL). Animal survival, weight loss, and clinical scores were monitored over 7 d post infection. The bacterial challenge was back-titrated to 4.33E8 CFU/mL and found within error range. Clinical scores are as defined: Score 1 (Healthy); 2 (Slightly Ruffled coat); 3 (Ruffled coat); 4 (Sick; walking but no scurrying); 5 (Very sick, closed inset eyes with slow to no movement); 6 (Moribund); 7 (Deceased).

Octet96 binning experiments

BLI measurements were made using Octet96 system (Forte Bio) which were pre-equipped with sensors for human/mouse anti-Fc sensors. Experimental details are provided in the Supplemental Appendix.

HDX-MS experiments

All reagents were procured from Sigma-Aldrich. Samples were digested online via a custom-packed pepsin column (2 × 20 mm) at room temperature. Post digestion, peptide trapping, and desalting were done by using a ZORBAX Eclipse XDB C8 column (2.1 × 15 mm, Agilent). After 3 min of desalting, peptides were separated on a reversed-phase C18 column (2.1 × 50 mm in size, 2.5 µm X select-CSH, Waters Corporation). Back exchange was minimized by placing the sample-handling components (valves, tubes, and column) in an ice slush during the digestion and HDX data collection. For LukF and Hla proteins, the eluted peptides were introduced to the mass spectrometer by electrospray ionization interfaced to an LTQ-FTICR mass spectrometer (Thermo Fisher) or a MaXis-4G quadrupole TOF instrument (Bruker Daltonics, Inc.). HDX experiments were conducted in duplicate unless otherwise noted. The data analysis was carried out using HDExaminer (version 2.5.0, Sierra Analytics, Inc., Modesto, CA).

Peptide mapping

Peptide mapping experiments were performed in non-deuterated PBS buffer pH = 7.4. Reversed-phase separated peptides were identified by collecting product-ion (MS/MS) spectra in a data-dependent mode. The six most abundant ions at any time were chosen in the LTQ-FTICR mass spectrometer and fragmented for default charge states from 1 to 4. For the MS/MS mode in the MaXis-4 G instrument, the cycle time was set as 3 s. The MS/MS data were analyzed utilizing Byonic and Byologic (Protein Metrics, San Carlos, CA). To discard a false-positive identification, data searches were performed against a reversed protein sequence.

Epitope mapping HDX experiments

LukF/antibody binding

A stock solution of 30 µM LukF was prepared by diluting in PBS (pH 7.4) buffer. LukF and antibodies SA02, SA131, and H5 were mixed in molar ratios of 1:2. LukF and the antibody SA185 were mixed in the molar ratio of 1:1.8. The mixtures were incubated at room temperature for 30 min before HDX measurements. HDX was initiated by diluting the reaction mixture 10-fold with deuterated PBS buffer. The samples were incubated several times (30, 60, 150, 300, 900, 1800, and 3600 s) at room temperature. The HDX was quenched with 4 M guanidine-hydrochloride, 200 mM TCEP, pH 2.5. Before quenching, 10 µL of 10 mg/mL Fungal XIII solution was added to the quenching solution. After 3 min of incubation, the samples were flash-frozen in liquid nitrogen and stored at -80°C until mass spectral analysis. Samples were quickly thawed and immediately injected into the LC/MS system, submitted to 3 min of online pepsin digestion and desalting. The flow rate was 200 µL/min comprised 0.1% trifluoroacetic acid aqueous solvent. Peptides were separated by using a chromatographic gradient with increasing organic solvent B (acetonitrile with 0.1% formic acid) from 5% to 100% over the 15 min.

Hla/antibody binding

The stock solution of 30 μ M Hla was prepared by diluting it in a PBS (pH 7.4) buffer. Hla and antibodies H5 and CAN6 were mixed in a molar ratio of 1:2. The mixture was incubated on ice for 1 h before HDX was initiated by diluting the reaction mixture 10-fold with deuterated PBS buffer. The samples were incubated at several time points (30, 60, 150, 300, 900, 1800, and 14400 s) on ice. The subsequent steps were the same as for LukF epitope mapping experiments. The peptides were corrected for back exchange using a fully deuterated protein state (FD). Proteins were fully deuterated by heating at 60°C overnight in deuterated buffer followed by its incubation for 2 d at room temperature. All HDX samples were processed in a Biosafety cabinet.

Statistical analysis

To measure the statistical differences in the deuterium uptake between two states, the cumulative differences in HDX for the bound (LukF + mAbs) versus unbound (LukF) were calculated. The cumulative differences were plotted along with the global significance limit.⁶⁴ We chose the statistical significance limit at $p < .01$ value to validate the statistical differences. Those differences showing a cumulative difference outside the significance limit were considered statistically significant changes.

Hla mutagenesis and purification

pET24 plasmids containing the mutant proteins were transformed into BL21(DE3) competent cells (Invitrogen™). Purification details are provided in the Supplemental Appendix.

Abbreviations

2B6	Hybridoma 2B6
ASN	Arsanis
ASN100	Cocktail of ASN-1 and ASN-2 monoclonal antibodies
AT62	Alpha toxin protein consisting of N terminal 62 amino acids
BCPFT	Bicomponent pore forming toxins
BLI	Bi-layer interferometry
bNAb (s)	Broadly neutralizing antibody/antibodies
CA	Community-associated
CAN6	Can24G4-1
CARB-X	Combating Antibiotic Resistant Bacteria Biopharmaceutical Accelerator
CFU	Colony Forming Unit
DMSO	Dimethyl sulfoxide
EC50	Half Maximal Effective constant (50%)
ELISA	Enzyme-linked immunoassay
FBS	Fetal bovine serum
FD	Fully deuterated protein state
H5	Arsanis-1 or Hla.F#5
HA	Hospital-associated
HDX-MS	Hydrogen/deuterium exchange mass spectrometry
Hla	α -hemolysin
HlgAB	γ -hemolysin AB
HlgCB	γ -hemolysin CB
Hu	Human
IACUC	Institutional Animal Care and Use Committee
IC50	Inhibition constant (50%)
IN	Intranasal
IP	Intraperitoneal

IPTG	Isopropyl β -D-1-thiogalactopyranoside
IsdB	Iron-regulated surface determinant system B
KD	Binding affinity
LC/MS	Liquid chromatography-mass spectrometry
LC10	Medi4893
LD100	Lethal dose (100%)
LMIC	Low- and middle-income countries
LTQ-FTICR	Linear ion trap-Fourier transform ion cyclotron resonance
LukAB	Leukocidin AB
LukED	Leukocidin ED
LukF-PV	Panton-valentine leukocidin f
LukSF-PV	Panton-Valentine leucocidin
LukS-PV	Panton-valentine leukocidin s
mAb(s)	Monoclonal antibody/antibodies
MEDI4893	Suvratoumab
MRSA	Multi-drug resistant Staphylococcus aureus
MS/MS	Tandem mass spectrometry
Mu	Murine
NT ₅₀	Neutralizing titer (50%)
OD	Optical density
PBS	phosphate buffered saline
PFT(s)	pore-forming toxin(s)
PMNs	Polymorphonuclear leukocytes
PVL	Panton-Valentine Leukocidin
RRBC	Rabbit red blood cell (s)
SA02	Staphylococcus aureus 02 monoclonal antibody
SA131	Staphylococcus aureus 131 monoclonal antibody
SA185	Staphylococcus aureus 185 monoclonal antibody
SASA	Solvent accessible surface area
SB	starting block buffer
SDS-PAGE	Sodium dodecyl-sulfate polyacrylamide gel electrophoresis
SEC-HPLC	size exclusion high performance liquid chromatography
SSTI	Skin and soft tissue infection
TCEP	tris(2-carboxyethyl)phosphine
TFA	trifluoroacetic acid
TOF	time of flight
TT	Beta turn
TTT	Alpha turn
VAP	Ventilator-associated pneumonia
WT	wild type

Disclosure statement

MA has stocks, and RA has stock options in Integrated Biotherapeutics Inc. The remaining authors declare that the research was conducted in the absence of any commercial or financial relationships that could be construed as a potential conflict of interest.

Funding

The research presented in this paper was supported by CARB-X. CARB-X's funding for this project is sponsored by the Cooperative Agreement Number IDSEP160030 from ASPR/BARDA and by awards from Wellcome Trust, the UK Global Antimicrobial Resistance Innovation Fund (GAMRIF), and the Bill & Melinda Gates Foundation. The content is solely the responsibility of the authors and does not necessarily represent the official views of CARB-X or any of its funders. Supported in part by NIH awards P01AI120943 and R01AI123926 to G.K.A and R01AI140758 to D.W.L. The mass spectrometry was supported by NHP41 GM103422 and R24 GM136766.

ORCID

Shweta Kailasan  <http://orcid.org/0000-0003-0876-6812>

References

- Wertheim HF, Melles DC, Vos MC, van Leeuwen W, van Belkum A, Verbrugh HA, Nouwen JL. The role of nasal carriage in *Staphylococcus aureus* infections. *Lancet Infect Dis*. 2005;5(12):751–62. doi:10.1016/S1473-3099(05)70295-4.
- Chambers HF, Deleo FR. Waves of resistance: *Staphylococcus aureus* in the antibiotic era. *Nat Rev Microbiol*. 2009;7(9):629–41. doi:10.1038/nrmicro2200.
- Shinefield H, Black S, Fattom A, Horwith G, Rasgon S, Ordonez J, Yeoh H, Law D, Robbins JB, Schneerson R, et al. Use of a *Staphylococcus aureus* conjugate vaccine in patients receiving hemodialysis. *N Engl J Med*. 2002;346(7):491–96. doi:10.1056/NEJMoa011297.
- Pozzi C, Wilk K, Lee JC, Gening M, Nifantiev N, Pier GB, Horsburgh MJ. Opsonic and protective properties of antibodies raised to conjugate vaccines targeting six *Staphylococcus aureus* antigens. *PLoS One*. 2012;7(10):e46648. doi:10.1371/journal.pone.0046648.
- Fowler VG, Allen KB, Moreira ED, Moustafa M, Isgro F, Boucher HW, Corey GR, Carmeli Y, Betts R, Hartzel JS, et al. Effect of an investigational vaccine for preventing *Staphylococcus aureus* infections after cardiothoracic surgery: a randomized trial. *JAMA*. 2013;309(13):1368–78. doi:10.1001/jama.2013.3010.
- Bennett MR, Bombardi RG, Kose N, Parrish EH, Nagel MB, Petit RA, Read TD, Schey KL, Thomsen IP, Skaar EP, et al. Human mAbs to *Staphylococcus aureus* IsdA provide protection through both heme-blocking and Fc-mediated mechanisms. *J Infect Dis*. 2019;219(8):1264–73. doi:10.1093/infdis/jiy635.
- Giersing BK, Dastgheyb SS, Modjarrad K, Moorthy V. Status of vaccine research and development of vaccines for *Staphylococcus aureus*. *Vaccine*. 2016;34(26):2962–66. doi:10.1016/j.vaccine.2016.03.110.
- Raafat D, Otto M, Reppschlagel K, Iqbal J, Holtfreter S. Fighting *Staphylococcus aureus* biofilms with monoclonal antibodies. *Trends Microbiol*. 2019;27(4):303–22. doi:10.1016/j.tim.2018.12.009.
- Fowler VG, Allen KB, Moreira ED, Moustafa M, Isgro F, Boucher HW, Corey GR, Carmeli Y, Betts R, Hartzel JS, et al. Effect of an investigational vaccine for preventing *Staphylococcus aureus* infections after cardiothoracic surgery. *JAMA*. 2013;309(13):1368.
- McNeely TB, Shah NA, Fridman A, Joshi A, Hartzel JS, Keshari RS, Lupu F, Dinubile MJ. Mortality among recipients of the Merck V710 *Staphylococcus aureus* vaccine after postoperative *S. aureus* infections: an analysis of possible contributing host factors. *Hum Vaccin Immunother*. 2014;10(12):3513–16. doi:10.4161/hv.34407.
- Karazum H, Haudenschild CC, Moore IN, Mahmoudieh M, Barber DL, Datta SK. Lethal CD4 T cell responses induced by vaccination against *Staphylococcus aureus* bacteremia. *J Infect Dis*. 2017;215(8):1231–39. doi:10.1093/infdis/jix096.
- Ragle BE, Bubeck Wardenburg J. Anti-alpha-hemolysin monoclonal antibodies mediate protection against *Staphylococcus aureus* pneumonia. *Infect Immun*. 2009;77(7):2712–18. doi:10.1128/IAI.00115-09.
- Ragle BE, Karginov VA, Bubeck Wardenburg J. Prevention and treatment of *Staphylococcus aureus* pneumonia with a β -cyclodextrin derivative. *Antimicrob Agents Chemother*. 2010;54(1):298–304. doi:10.1128/AAC.00973-09.
- Rouha H, Badarau A, Visram ZC, Battles MB, Prinz B, Magyarics Z, Nagy G, Mirkina I, Stulik L, Zerbs M, et al. Five birds, one stone: neutralization of α -hemolysin and 4 bi-component leukocidins of *Staphylococcus aureus* with a single human monoclonal antibody. *MABS*. 2015;7(1):243–54. doi:10.4161/19420862.2014.985132.
- Diep BA, Le VT, Visram ZC, Rouha H, Stulik L, Dip EC, Nagy G, Nagy E. Improved protection in a rabbit model of community-associated methicillin-resistant *Staphylococcus aureus* necrotizing pneumonia upon neutralization of leukocidins in addition to alpha-hemolysin. *Antimicrob Agents Chemother*. 2016;60(10):6333–40. doi:10.1128/AAC.01213-16.
- Guillet V, Roblin P, Werner S, Coraiola M, Menestrina G, Monteil H, Prevost G, Mourey L. Crystal structure of leucotoxin S component: new insight into the *Staphylococcal* beta-barrel pore-forming toxins. *J Biol Chem*. 2004;279(39):41028–37. doi:10.1074/jbc.M406904200.
- Prevost G, Couppie P, Prevost P, Gayet S, Petiau P, Cribier B, Monteil H, Piemont Y. Epidemiological data on *Staphylococcus aureus* strains producing synergohymenotropic toxins. *J Med Microbiol*. 1995;42(4):237–45. doi:10.1099/00222615-42-4-237.
- Spaan AN, van Strijp Jag, Torres VJ, van Strijp JAG. Leukocidins: staphylococcal bi-component pore-forming toxins find their receptors. *Nat Rev Microbiol*. 2017;15(7):435–47. doi:10.1038/nrmicro.2017.27.
- Berube BJ, Bubeck Wardenburg J. *Staphylococcus aureus* α -Toxin: nearly a century of intrigue. *Toxins (Basel)*. 2013;5(6):1140–66. doi:10.3390/toxins5061140.
- Song L, Hobaugh MR, Shustak C, Cheley S, Bayley H, Gouaux JE. Structure of staphylococcal alpha-hemolysin, a heptameric transmembrane pore. *Science*. 1996;274(5294):1859–66. doi:10.1126/science.274.5294.1859.
- Aman MJ, Adhikari RP. Staphylococcal bicomponent pore-forming toxins: targets for prophylaxis and immunotherapy. *Toxins (Basel)*. 2014;6(3):950–72. doi:10.3390/toxins6030950.
- Pedelaq JD, Maveyraud L, Prevost G, Baba-Moussa L, Gonzalez A, Courcelle E, Shepard W, Monteil H, Samama JP, Mourey L. The structure of a *Staphylococcus aureus* leukocidin component (LukF-PV) reveals the fold of the water-soluble species of a family of transmembrane pore-forming toxins. *Structure*. 1999;7(3):277–87. doi:10.1016/S0969-2126(99)80038-0.
- Morinaga N, Kaihou Y, Noda MP. Cloning and characterization of variant LukE-LukD with strong leukocidal activity of staphylococcal Bi-component leukotoxin family. *Microbiol Immunol*. 2003;47(1):81–90. doi:10.1111/j.1348-0421.2003.tb02789.x.
- Ventura CL, Malachowa N, Hammer CH, Nardone GA, Robinson MA, Kobayashi SD, DeLeo FR, Horsburgh MJ. Identification of a novel *Staphylococcus aureus* two-component leukotoxin using cell surface proteomics. *PLoS One*. 2010;5(7):e11634. doi:10.1371/journal.pone.0011634.
- Shukla SK, Karow ME, Brady JM, Stemper ME, Kislow J, Moore N, Wroblewski K, Chyou PH, Warshauer DM, Reed KD, et al. Virulence genes and genotypic associations in nasal carriage, community-associated methicillin-susceptible and methicillin-resistant USA400 *Staphylococcus aureus* isolates. *J Clin Microbiol*. 2010;48(10):3582–92. doi:10.1128/JCM.00657-10.
- Wang R, Braughton KR, Kretschmer D, Bach TH, Queck SY, Li M, Kennedy AD, Dorward DW, Klebanoff SJ, Peschel A, et al. Identification of novel cytolytic peptides as key virulence determinants for community-associated MRSA. *Nat Med*. 2007;13(12):1510–14. doi:10.1038/nm1656.
- Li M, Diep BA, Villaruz AE, Braughton KR, Jiang X, DeLeo FR, Chambers HF, Lu Y, Otto M. Evolution of virulence in epidemic community-associated methicillin-resistant *Staphylococcus aureus*. *Proc Natl Acad Sci U S A*. 2009;106(14):5883–88. doi:10.1073/pnas.0900743106.
- Wardenburg JB, Schneewind O. Vaccine protection against *Staphylococcus aureus* pneumonia. *J Exp Med*. 2008;205(2):287–94. doi:10.1084/jem.20072208.
- Darboe S, Dobreniecki S, Jarju S, Jallow M, Mohammed NI, Wathuo M, Ceesay B, Tweed S, Basu Roy R, Okomo U, et al. Prevalence of Pantone-Valentine Leukocidin (PVL) and antimicrobial resistance in community-acquired clinical *Staphylococcus aureus* in an urban Gambian hospital: a 11-year period retrospective pilot study. *Front Cell Infect Microbiol*. 2019;9:170. doi:10.3389/fcimb.2019.00170.
- DeLeo FR, Otto M, Kreiswirth BN, Chambers HF. Community-associated methicillin-resistant *Staphylococcus aureus*. *Lancet*. 2010;375(9725):1557–68. doi:10.1016/S0140-6736(09)61999-1.

31. Nhan TX, Leclercq R, Cattoir V. Prevalence of toxin genes in consecutive clinical isolates of *Staphylococcus aureus* and clinical impact. *Eur J Clin Microbiol Infect Dis*. 2011;30(6):719–25. doi:10.1007/s10096-010-1143-4.
32. Vandenesch F, Naimi T, Enright MC, Lina G, Nimmo GR, Heffernan H, Liassine N, Bes M, Greenland T, Reverdy ME, et al. Community-acquired methicillin-resistant *Staphylococcus aureus* carrying panton-valentine leukocidin genes: worldwide emergence. *Emerg Infect Dis*. 2003;9(8):978–84. doi:10.3201/eid0908.030089.
33. Tristan A, Bes M, Meugnier H, Lina G, Bozdogan B, Courvalin P, Reverdy ME, Enright MC, Vandenesch F, Etienne J. Global distribution of panton-valentine leukocidin-positive methicillin-resistant *Staphylococcus aureus*, 2006. *Emerg Infect Dis*. 2007;13(4):594–600. doi:10.3201/eid1304.061316.
34. Lina G, Piemont Y, Godail-Gamot F, Bes M, Peter MO, Gauduchon V, Vandenesch F, Etienne J. Involvement of Panton-Valentine leukocidin-producing *Staphylococcus aureus* in primary skin infections and pneumonia. *Clin Infect Dis*. 1999;29(5):1128–32. doi:10.1086/313461.
35. Gillet Y, Issartel B, Vanhems P, Fournet JC, Lina G, Bes M, Vandenesch F, Piemont Y, Brousse N, Floret D, et al. Association between *Staphylococcus aureus* strains carrying gene for panton-valentine leukocidin and highly lethal necrotising pneumonia in young immunocompetent patients. *Lancet*. 2002;359(9308):753–59. doi:10.1016/S0140-6736(02)07877-7.
36. Bocchini CE, Hulten KG, Mason EO Jr., Gonzalez BE, Hammerman WA, Kaplan SL. Panton-valentine leukocidin genes are associated with enhanced inflammatory response and local disease in acute hematogenous *Staphylococcus aureus* osteomyelitis in children. *Pediatrics*. 2006;117(2):433–40. doi:10.1542/peds.2005-0566.
37. Adhikari RP, Ajao AO, Aman MJ, Karauzum H, Sarwar J, Lydecker AD, Johnson JK, Nguyen C, Chen WH, Roghmann MC. Lower antibody levels to *Staphylococcus aureus* exotoxins are associated with sepsis in hospitalized adults with invasive *S. aureus* infections. *J Infect Dis*. 2012;206(6):915–23. doi:10.1093/infdis/jis462.
38. Fritz SA, Tiemann KM, Hogan PG, Epplin EK, Rodriguez M, Al-Zubeidi DN, Bubeck-Wardenburg J, Hunstad DA. A serologic correlate of protective immunity against community-onset *Staphylococcus aureus* infection. *Clin Infect Dis*. 2013;56(11):1554–61. doi:10.1093/cid/cit123.
39. Hua L, Hilliard JJ, Shi Y, Tkaczyk C, Cheng LI, Yu X, Datta V, Ren S, Feng H, Zinsou R, et al. Assessment of an anti-alpha-toxin monoclonal antibody for prevention and treatment of *Staphylococcus aureus*-induced pneumonia. *Antimicrob Agents Chemother*. 2014;58(2):1108–17. doi:10.1128/AAC.02190-13.
40. Hua L, Cohen TS, Shi Y, Datta V, Hilliard JJ, Tkaczyk C, Suzich J, Stover CK, Sellman BR. MEDI4893* promotes survival and extends the antibiotic treatment window in a *staphylococcus aureus* immunocompromised pneumonia model. *Antimicrob Agents Chemother*. 2015;59(8):4526–32. doi:10.1128/AAC.00510-15.
41. Venkatasubramanian A, Kanipakala T, Ganjbaksh N, Mehr R, Mukherjee I, Krishnan S, Bae T, Aman MJ, Adhikari RP. A critical role for HlgA in *Staphylococcus aureus* pathogenesis revealed by A switch in the SaeRS two-component regulatory system. *Toxins (Basel)*. 2018;10(9):377. doi:10.3390/toxins10090377.
42. Zp, K M, Adi N, Czarnik T, Japaridze K, Kartsivadze N, Kirov M, Campanaro E, Muir L, Kollef MH, Stevens C, et al. Results of a phase 2, randomized, double-blind, placebo-controlled study to determine the safety and efficacy of a single dose of the monoclonal antibody combination ASN100 for the prevention of *Staphylococcus aureus* pneumonia in endotracheal heavily colonized, mechanically ventilated subjects. In Proceedings of the 29th Meeting of the European Society of Microbiology and Infectious Diseases (ECCMID); 2019.
43. Keck Z-Y, Xia J, Wang Y, Wang W, Krey T, Prentoe J, Carlsen T, Li AY, Patel AH, Lemon SM, et al. Human monoclonal antibodies to a novel cluster of conformational epitopes on HCV E2 with resistance to neutralization escape in a genotype 2a isolate. *PLoS Pathog*. 2012;8(4):e1002653. doi:10.1371/journal.ppat.1002653.
44. Jody Berry LS, Cassan R, Han X, Javad Aman M, Rajan PA, Karauzum H. *Staphylococcus aureus* alpha-hemolysin antibodies. USA; 2012.
45. Amatya P, Wagner N, Chen G, Luthra P, Shi L, Borek D, Pavlenko A, Rohrs H, Basler CF, Sidhu SS, et al. Inhibition of Marburg virus RNA synthesis by a synthetic Anti-VP35 antibody. *ACS Infect Dis*. 2019;5(8):1385–96. doi:10.1021/acscinfdis.9b00091.
46. Chen G, Karauzum H, Long H, Carranza D, Holtsberg FW, Howell KA, Abaandou L, Zhang B, Jarvik N, Ye W, et al. Potent neutralization of *Staphylococcal* enterotoxin B in vivo by antibodies that block binding to the T-cell receptor. *J Mol Biol*. 2019;1.
47. Olson R, Nariya H, Yokota K, Kamio Y, Gouaux E. Crystal structure of *Staphylococcal* LukF delineates conformational changes accompanying formation of a transmembrane channel. *Nat Struct Biol*. 1999;6(2):134–40. doi:10.1038/5821.
48. Badarau A, Rouha H, Malafa S, Battles MB, Nielson N, Dolezilskova I, Teubenbacher A, Maierhofer B, Weber S, Stulik L, et al. Context matters: the importance of dimerization-induced conformation of the LukGH leukocidin of *Staphylococcus aureus* for the generation of neutralizing antibodies. *mAbs*. 2016;8(7):1347–60. doi:10.1080/19420862.2016.1215791.
49. Sugawara T, Yamashita D, Kato K, Peng Z, Ueda J, Kaneko J, Kamio Y, Tanaka Y, Yao M. Structural basis for pore-forming mechanism of staphylococcal α -hemolysin. *Toxicon*. 2015;108:226–31. doi:10.1016/j.toxicon.2015.09.033.
50. Robert X, Gouet P. Deciphering key features in protein structures with the new ENDscript server. *Nucleic Acids Research*. 2014;42(W1):W320–W324. doi:10.1093/nar/gku316.
51. Oganasyan V, Peng L, Damschroder MM, Cheng L, Sadowska A, Tkaczyk C, Sellman BR, Wu H, Dall'Acqua WF. Mechanisms of neutralization of a human anti- α -toxin antibody. *J Biol Chem*. 2014;289(43):29874–80. doi:10.1074/jbc.M114.601328.
52. Tkaczyk C, Semenova E, Shi YY, Rosenthal K, Oganasyan V, Warren P, Stover CK, Sellman BR. Alanine scanning mutagenesis of the MEDI4893 (Suvratoxumab) epitope reduces alpha toxin lytic activity in vitro and *Staphylococcus aureus* fitness in infection models. *Antimicrob Agents Chemother*. 2018;62.
53. Tabor DE, Yu L, Mok H, Tkaczyk C, Sellman BR, Wu Y, Oganasyan V, Slidel T, Jafri H, McCarthy M, et al. *Staphylococcus aureus* alpha-toxin is conserved among diverse hospital respiratory isolates collected from a global surveillance study and is neutralized by monoclonal antibody MEDI4893. *Antimicrob Agents Chemother*. 2016;60:5312–21.
54. Pettersen E F, Goddard T D, Huang C C, Couch G S, Greenblatt D M, Meng E C, Ferrin T E. UCSF Chimera?A visualization system for exploratory research and analysis. *J. Comput. Chem*. 2004;25(13):1605–1612. doi:10.1002/jcc.20084.
55. McWilliam H, Li W, Uludag M, Squizzato S, Park Y Mi, Buso N, Cowley A Peter, Lopez R. Analysis Tool Web Services from the EMBL-EBI. *Nucleic Acids Res*. 2013;41(Web Server issue):W597–600. doi:10.1093/nar/gkt376.
56. Speziale P, Pietrocola G. Monoclonal Antibodies Targeting Surface-Exposed and Secreted Proteins from *Staphylococci*. *Vaccines (Basel)*. 2021;9(5). doi:10.3390/vaccines9050459.
57. Tam K, Torres VJ, Fischetti VA, Novick RP, Ferretti JJ, Portnoy DA, Braunstein M, Rood JJ. *Staphylococcus aureus* secreted toxins and extracellular enzymes. *Microbiol Spectr*. 2019;7(2). doi:10.1128/microbiolspec.GPP3-0039-2018.
58. Valeva A, Pongs J, Bhakdi S, Palmer M. *Staphylococcal* alpha-toxin : the role of the N-terminus in formation of the heptameric pore – a fluorescence study. *Biochim Biophys Acta*. 1997;1325(2):281–86. doi:10.1016/S0005-2736(96)00266-0.

59. Adhikari RP, Karauzum H, Sarwar J, Abaandou L, Mahmoudieh M, Boroun AR, Vu H, Nguyen T, Devi VS, Shulenin S, et al. Novel structurally designed vaccine for *S. aureus* alpha-hemolysin: protection against bacteremia and pneumonia. *PLoS One*. 2012;7(6):e38567. doi:10.1371/journal.pone.0038567.
60. Walker B, Bayley H. Key residues for membrane binding, oligomerization, and pore forming activity of staphylococcal alpha-hemolysin identified by cysteine scanning mutagenesis and targeted chemical modification. *J Biol Chem*. 1995;270:23065–71. doi:10.1074/jbc.270.39.23065.
61. Peraro MD, Van Der Goot FG. Pore-forming toxins: ancient, but never really out of fashion. *Nat Rev Microbiol*. 2016;14(2):77–92. doi:10.1038/nrmicro.2015.3.
62. Song L, Hobaugh MR, Shustak C, Cheley S, Gouaux JE. Structure of Staphylococcal α -hemolysin, a heptameric transmembrane pore published by: American Association for the Advancement of Science. Stable URL: <http://www.jstor.org/stable/2891686>. *Science* 1996; 274:1859–66.
63. Adhikari RP, Thompson CD, Aman MJ, Lee JC. Protective efficacy of a novel alpha hemolysin subunit vaccine (AT62) against *Staphylococcus aureus* skin and soft tissue infections. *Vaccine*. 2016;34:6402–07.
64. Hageman TS, Weis DD. Reliable identification of significant differences in differential hydrogen exchange-mass spectrometry measurements using a hybrid significance testing approach. *Anal Chem*. 2019;91(13):8008–16. doi:10.1021/acs.analchem.9b01325.